

AD_____

Award Number: W81XWH-06-1-0462

TITLE: Optimization and Comparison of Different Digital Mammographic
Tomosynthesis Reconstruction Methods

PRINCIPAL INVESTIGATOR: Ying Chen, Ph.D.
James T. Dobbins III, Ph.D. (Mentor)

CONTRACTING ORGANIZATION: Duke University
Durham, North Carolina, 27710

REPORT DATE: April 2008

TYPE OF REPORT: Annual Summary

PREPARED FOR: U.S. Army Medical Research and Materiel Command
Fort Detrick, Maryland 21702-5012

DISTRIBUTION STATEMENT: Approved for Public Release;
Distribution Unlimited

The views, opinions and/or findings contained in this report are those of the author(s) and should not be construed as an official Department of the Army position, policy or decision unless so designated by other documentation.

REPORT DOCUMENTATION PAGE				<i>Form Approved</i> OMB No. 0704-0188	
Public reporting burden for this collection of information is estimated to average 1 hour per response, including the time for reviewing instructions, searching existing data sources, gathering and maintaining the data needed, and completing and reviewing this collection of information. Send comments regarding this burden estimate or any other aspect of this collection of information, including suggestions for reducing this burden to Department of Defense, Washington Headquarters Services, Directorate for Information Operations and Reports (0704-0188), 1215 Jefferson Davis Highway, Suite 1204, Arlington, VA 22202-4302. Respondents should be aware that notwithstanding any other provision of law, no person shall be subject to any penalty for failing to comply with a collection of information if it does not display a currently valid OMB control number. PLEASE DO NOT RETURN YOUR FORM TO THE ABOVE ADDRESS.					
1. REPORT DATE (DD-MM-YYYY) 01-04-2008		2. REPORT TYPE Annual Summary		3. DATES COVERED (From - To) 31 MAR 2006 - 30 MAR 2008	
4. TITLE AND SUBTITLE Optimization and Comparison of Different Digital Mammographic Tomosynthesis Reconstruction Methods				5a. CONTRACT NUMBER	
				5b. GRANT NUMBER W81XWH-06-1-0462	
				5c. PROGRAM ELEMENT NUMBER	
6. AUTHOR(S) Ying Chen, Ph.D.; James T. Dobbins III, Ph.D. E-Mail: chen@engr.siu.edu				5d. PROJECT NUMBER	
				5e. TASK NUMBER	
				5f. WORK UNIT NUMBER	
7. PERFORMING ORGANIZATION NAME(S) AND ADDRESS(ES) Duke University Durham, North Carolina, 27710				8. PERFORMING ORGANIZATION REPORT NUMBER	
9. SPONSORING / MONITORING AGENCY NAME(S) AND ADDRESS(ES) U.S. Army Medical Research and Materiel Command Fort Detrick, Maryland 21702-5012				10. SPONSOR/MONITOR'S ACRONYM(S)	
				11. SPONSOR/MONITOR'S REPORT NUMBER(S)	
12. DISTRIBUTION / AVAILABILITY STATEMENT Approved for Public Release; Distribution Unlimited					
13. SUPPLEMENTARY NOTES					
14. ABSTRACT Digital breast tomosynthesis is a three-dimensional imaging technique with limited-angle series of projection images that allows the reconstruction of depth information along the breast. This study investigated, optimized and compared different tomosynthesis methods and chose the optimal one for breast tomosynthesis imaging. We investigated several 3-D tomosynthesis reconstruction algorithms and studied the effect of acquisition parameters for different candidate reconstruction algorithms, according to computer simulation and physical measurements of impulse response analysis, modulation transfer function and noise power spectrum. We applied a relative noise-equivalent quanta (NEQ) analysis to compare candidate algorithms and acquisition parameters. Additionally, the importance of point-by-point back projection (BP) for isocentric motion in breast tomosynthesis was investigated. It improves the in-plane sharpness of structures such as microcalcifications, which bear important meaning in clinical tasks for breast cancer detection.					
15. SUBJECT TERMS mammography, tomosynthesis, noise power spectrum (NPS), modulation transfer function (MTF), shift-add-add (SAA), back projection (BP), filtered back projection (FBP), matrix inversion tomosynthesis (MITS), maximum likelihood expectation maximization (MLEM), Gaussian frequency blending (GFB)					
16. SECURITY CLASSIFICATION OF:			17. LIMITATION OF ABSTRACT UU	18. NUMBER OF PAGES 41	19a. NAME OF RESPONSIBLE PERSON USAMRMC
a. REPORT U	b. ABSTRACT U	c. THIS PAGE U			19b. TELEPHONE NUMBER (include area code)

Table of Contents

	<u>Page</u>
Patent Report.....	4
Termination Request.....	5
Introduction.....	6
Body.....	6
Key Research Accomplishments.....	13
Reportable Outcomes.....	14
Conclusions.....	14
References.....	15
Appendices.....	17

REPORT OF INVENTIONS AND SUBCONTRACTS
(Pursuant to "Patent Rights" Contract Clause) (See Instructions on back)

Form Approved
OMB No. 9000-0095
Expires Jan 31, 2008

The public reporting burden for this collection of information is estimated to average 1 hour per response, including the time for reviewing instructions, searching existing data sources, gathering and maintaining the data needed, and completing and reviewing the collection of information. Send comments regarding this burden estimate or any other aspect of this collection of information, including suggestions for reducing the burden, to the Department of Defense, Executive Services Directorate (9000-0095). Respondents should be aware that notwithstanding any other provision of law, no person shall be subject to any penalty for failing to comply with a collection of information if it does not display a currently valid OMB control number.

PLEASE DO NOT RETURN YOUR COMPLETED FORM TO THE ABOVE ORGANIZATION. RETURN COMPLETED FORM TO THE CONTRACTING OFFICER.

1.a. NAME OF CONTRACTOR/SUBCONTRACTOR
DUKE UNIVERSITY
334 NORTH BUILDING
DURHAM, NC 27708

1.b. ADDRESS (Include ZIP Code)
334 NORTH BUILDING
DURHAM, NC 27708

1.c. CONTRACT NUMBER
WRXWH-06-1-0442

1.d. AWARD DATE (YYYYMMDD)
20060321

2.a. NAME OF GOVERNMENT PRIME CONTRACTOR

2.b. ADDRESS (Include ZIP Code)

2.c. CONTRACT NUMBER

2.d. AWARD DATE (YYYYMMDD)

3. TYPE OF REPORT (X one)
a. INTERIM
b. FINAL

4. REPORTING PERIOD (YYYYMMDD)
a. FROM 20060401
b. TO 20070901

5. "SUBJECT INVENTIONS" REQUIRED TO BE REPORTED BY CONTRACTOR/SUBCONTRACTOR (If "None," so state)

NAME(S) OF INVENTOR(S)
(Last, First, Middle Initial)
CHEN, YING

TITLE OF INVENTION(S)
None.

DISCLOSURE NUMBER, PATENT APPLICATION SERIAL NUMBER OR PATENT NUMBER
c.

ELECTION TO FILE PATENT APPLICATIONS (X)
d.
(1) UNITED STATES (a) YES (b) NO
(2) FOREIGN (a) YES (b) NO

CONFIRMATORY INSTRUMENT OR ASSIGNMENT FORWARDED TO CONTRACTING OFFICER (X)
e.
(a) YES (b) NO

6. SUBCONTRACTS AWARDED BY CONTRACTOR/SUBCONTRACTOR (If "None," so state)

NAME OF SUBCONTRACTOR(S)
a.

ADDRESS (Include ZIP Code)
b.

1. (a) NAME OF INVENTOR (Last, First, Middle Initial)
(2) (a) NAME OF INVENTOR (Last, First, Middle Initial)
(b) NAME OF EMPLOYER
(c) ADDRESS OF EMPLOYER (Include ZIP Code)

2. (1) TITLE OF INVENTION
(2) FOREIGN COUNTRIES OF PATENT APPLICATION

DESCRIPTION OF WORK TO BE PERFORMED UNDER SUBCONTRACT(S)
e.

FAR "PATENT RIGHTS"
d.
(1) CLAUSE NUMBER
(2) DATE (YYYYMM)

SUBCONTRACT NUMBER(S)
c.

SUBCONTRACT DATES (YYYYMMDD)
f.
(1) AWARD
(2) ESTIMATED COMPLETION

7. CERTIFICATION OF REPORT BY CONTRACTOR/SUBCONTRACTOR (Not required if: (X as appropriate))

NAME OF AUTHORIZED CONTRACTOR/SUBCONTRACTOR OFFICIAL (Last, First, Middle Initial)
Scripa, Maria

TITLE
Assistant Director

SIGNATURE
Maria Scripa

DATE SIGNED
8/14/07

8. I certify that the reporting party has procedures for prompt identification and timely disclosure of "Subject Inventions," that such procedures have been followed and that all "Subject Inventions" have been reported.

SMALL BUSINESS or

NONPROFIT ORGANIZATION

DD FORM 882, JUL 2005

Office of Preaward Subcontracting
Duke University

FORMFLOW/Adobe Professional 6.0

August 13, 2007

Ms. Pamela L. Fisher, Contracting/Grant Officer
Department of the Army
United States Army Medical Research Acquisition Activity

Dear Ms. Fisher:

Please accept this letter as my formal request to withdraw from contract number W81XWH-06-1-0462, effective September 1, 2007. I have received my PhD from Duke University.

Thank you for allowing me this opportunity. If you should need additional information, please contact me.

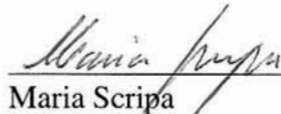
Sincerely,

Ying Chen



829 Louise Circle
Durham, NC 27705

Email: adachen@duke.edu



Maria Scripa
Assistant Director
Office of Research Support

8/14/07
Date

INTRODUCTION

This study investigated a novel imaging technology of digital breast tomosynthesis (DBT) to improve early breast cancer detection.

Breast cancer is a major problem and the most common cancer among women. Approximately over 10% of women in the US will develop breast cancer during their lifetime^{1, 2} and 30% to 40% of American women who get breast cancer die from it.¹ Annually, a total of 348,000 cases of breast cancer is diagnosed and almost 115,000 are killed by breast cancer in the US and European Community.² Mammography is currently the most important and efficacious tool for the early detection of breast cancer.³ However, the nature of the two-dimensional mammography makes it very difficult to distinguish a cancer from overlying breast tissues, especially for dense breast cases.

Digital breast tomosynthesis is a three-dimensional breast imaging method to reconstruct a set of planes in the breast from limited-angle series of projection images as the x-ray source. A variety of tomosynthesis reconstruction algorithms have been proposed including the traditional shift-and-add (SAA), the image-stretching method proposed by Nilklason and colleagues⁴, the maximum likelihood iterative algorithm (MLEM) by Wu et al.^{5, 6}, tuned-aperture computed tomography (TACT) reconstruction methods developed by Webber and investigated by Suryanarayanan *et al*^{7, 8}, algebraic reconstruction techniques (ART)⁹⁻¹¹, filtered back projection (FBP)¹²⁻¹⁶, and matrix inversion tomosynthesis (MITS)¹⁶⁻¹⁸.

The purpose of this project is to optimize and compare several different tomosynthesis reconstruction algorithms that are either initially investigated in our lab or currently very popular, and to optimize the imaging acquisition techniques. Based on this project, we hope to contribute to the optimal breast tomosynthesis technique for better breast cancer detection.

Note that although this predoctoral fellowship was awarded for two years, it has now been concluded in one year and five months. The recipient, Ying Chen, just graduated in August 2007 and has resigned from the fellowship. The fellowship provided her with a solid foundation in cancer research and has allowed her to continue with cancer research as a tenure-track assistant professor at Southern Illinois University.

BODY

Task 1. Optimization of different candidate tomosynthesis reconstruction methods (Month 1-12):

1.1. Select candidate algorithms from different algorithm families for optimization and comparison. 2-4 candidate algorithms from different algorithm families will be chosen. (Month 1-4).

This task has been completed and has resulted in publications (see #1, #2 and #3 in Reportable Outcomes). We have investigated a few reconstruction algorithms, including shift-and-add (SAA) algorithm, Nilklason's image stretching shift-and-add (NIKL), maximum likelihood expectation maximization (MLEM), matrix inversion tomosynthesis (MITS), and filtered back projection (FBP).

Among those algorithms, MITS was originally invented in our lab by Dobbins¹⁸ and we applied it to the breast tomosynthesis imaging successfully^{16, 17}. We also developed our FBP reconstruction based on central slice theorem and Fourier frequency sampling density. In order to control the high frequency noise amplification, Hamming Gaussian filters were designed and applied to our FBP algorithm^{16, 19}. MLEM algorithm is an effective iterative method in breast tomosynthesis reconstruction. However, it is time-consuming due to intensive computation. Therefore, in this project, we selected back projection (BP), MITS and FBP as our three candidate algorithms for comparison and optimization. But we also did related research on other algorithms such as SAA, NIKL, and MLEM.

During our investigation of different algorithms, we found that quite a few other algorithms depend on a traditional SAA method. However, a simple SAA reconstruction algorithm is not entirely suitable for isocentric motion in breast tomosynthesis, especially for small structures such as microcalcifications, which have an important bearing in clinical breast cancer detection tasks. A point-by-point back projection (BP) is important for isocentric motion in breast tomosynthesis.

We have published our results in *Medical Physics*, the premiere peer-reviewed journal in the field of Medical Physics; please see Appendix #1 for the reprinted publication.

1.2. Characterize the effect of three acquisition parameters including total Tomographic-Angle (TA), Number of projection images (N), and Reconstruction-Slice-Spacing (RSS) for each reconstruction algorithm, according to physical measurements of impulse response analysis, modulation transfer function (MTF) and noise power spectrum (NPS). (Months 5-12).

This task has been completed and has resulted in publications (see #1, #2, #3, and #4) in Reportable Outcomes). Parameters of a selenium-based direct conversion Siemens Mammomat Novation DR prototype system was modified to be used for geometries of the simulation. Seven different combinations of acquisition parameters were investigated. We have characterized candidate algorithms and different combinations of acquisition parameters by simulation and physical measurements of impulse response, MTF and NPS.

For each combination of acquisition parameters, datasets of tomosynthesis projection sequences with several different impulse locations were simulated with a ray-tracing method and then reconstructed with candidate tomosynthesis algorithms. Impulse response was analyzed and compared. We have measured MTF values of each algorithm and acquisition parameters based on two parts: 1) measured system MTF of the detector by previously published edge-method^{20, 21}; 2) the relative reconstruction MTF associated with specific reconstruction algorithm and acquisition parameters. For MITS and FBP algorithms, due to applied deblurring algorithms, there is no real meaningful DC components to normalize the MTF. Therefore, we calculated relative reconstruction MTF as the magnitude of Fourier Transform of the impulse response associated with specific reconstruction algorithm and acquisition parameters.

In order to compute the noise power spectrum (NPS) for specific acquisition parameters, two identical phantom slabs (47% water/ 53% adipose equivalent) for a total of 4 cm thickness were put directly on the surface plate (detector cover) to mimic the breast tissue equivalent attenuation and scattered radiation. Ten identical tomosynthesis sequences of flat images with the phantom slabs on the detector were acquired. The tomosynthesis sequences were then reconstructed by each candidate algorithm. Mean-subtracted NPS was analyzed to remove fixed pattern noise, including structured noise and system artifacts.^{22, 23}

Figures 1(a), 1(b) and 1(c) show an example of in-plane impulse response analysis for BP, MITS and FBP algorithms respectively with 25 projection images and $\pm 25^\circ$ total tomographic angle of x-ray tube's movement. The impulse was located 25 mm above the detector cover surface plate and near the chest wall.

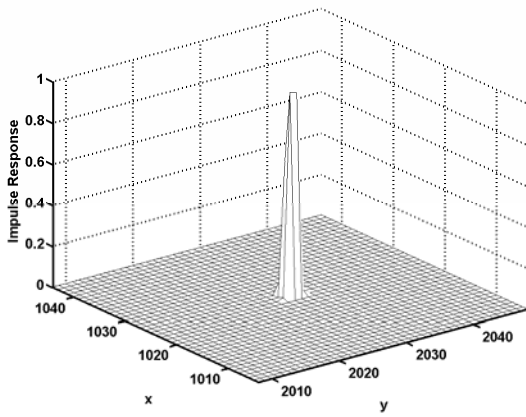


Figure 1(a): Impulse response example of BP

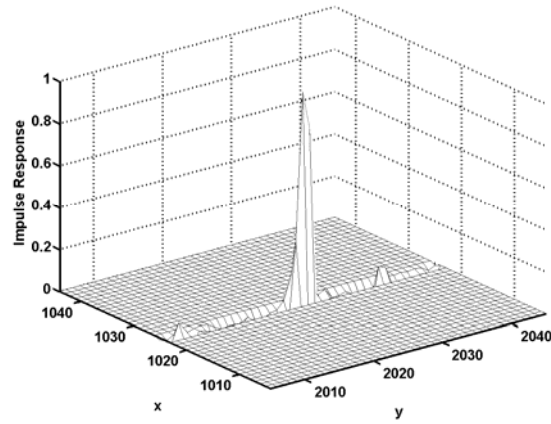


Figure 1(b): Impulse response example of MITS

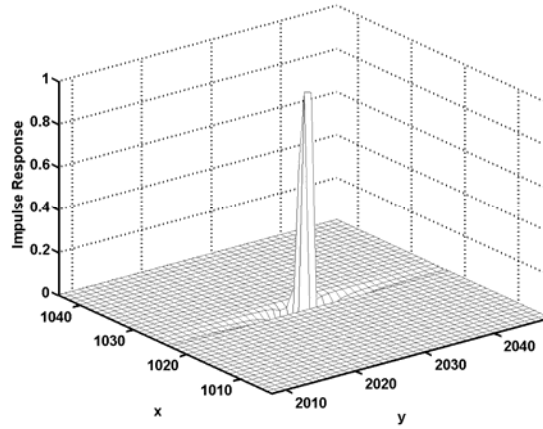


Figure 1(c): Impulse response example of FBP

We found that all three algorithms can reconstruct the simulated impulses to give sharp in-plane responses. MITS and FBP have tails due to their edge enhancement effects. For out-of-plane response, compared with BP, MITS and FBP were always better for removal of out-of-plane blur artifacts. There was no substantial difference for BP with different acquisition parameters. For MITS and FBP, bigger N cases were better in high frequency noise removal. FBP performed better with wider tomographic angle of tube's movement. For MITS, when impulse is located

near chest wall and with a narrower tomographic angle, MITS performed well with less artifacts associated with isocentric motion of breast tomosynthesis.

Figures 2(a), 2(b) and 2(c) show an example of our relative MTF analysis of BP, MITS and FBP, respectively, with seven different combinations of acquisition parameters. Acquisition parameters were named based on tomographic angle (TA) and number of projection images (N) for clarity. Scrub (“Bo”) means a simple dark current image between each frame. Binning mode (“Bin”) means to sum up the neighboring 2 pixel values along the x-ray tube’s motion to speed up the tomosynthesis scan. For examples, B0-bin-A50-P25 means: Angular range = 50° , Projection images = 25, with “Bo” scrub and Binning mode; A44-P13 means: Angular range = 44° , Projection images = 13.

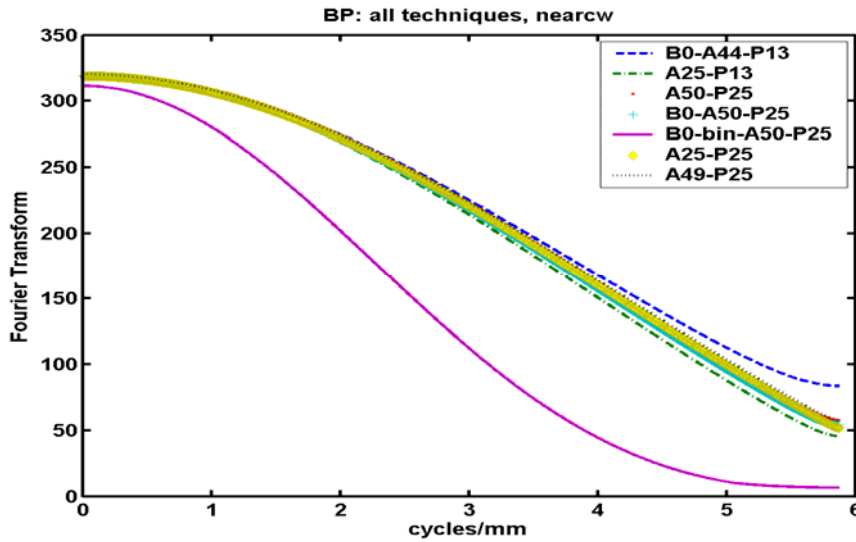


Figure 2(a): Relative MTF of BP for several different acquisition combinations

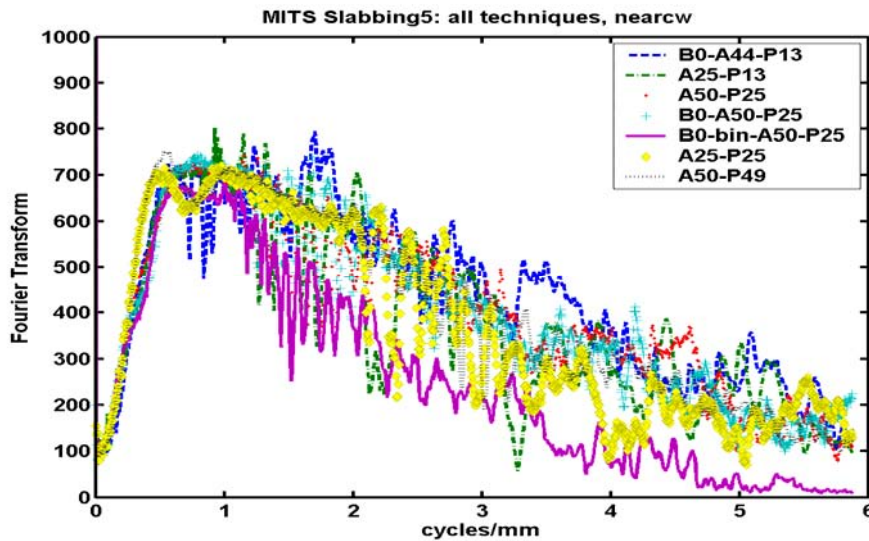


Figure 2(b): Relative MTF of MITS for several different acquisition combinations

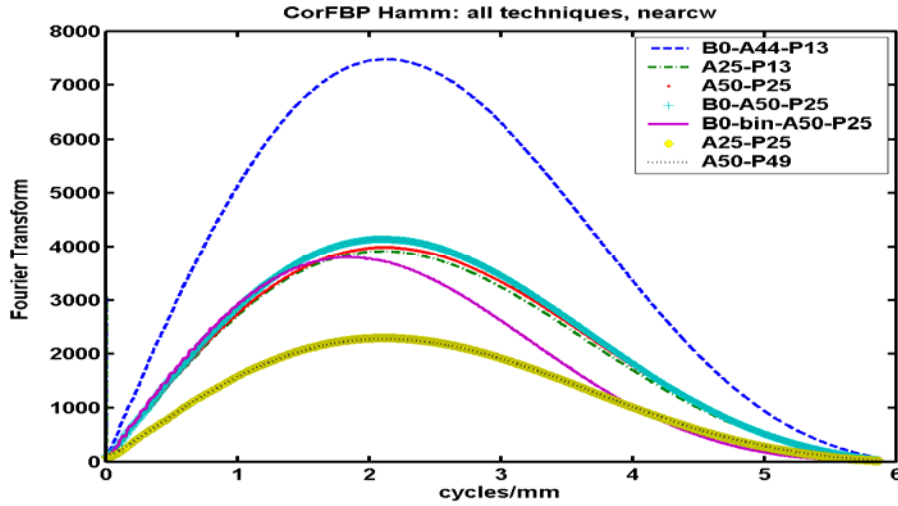


Figure 2(c): Relative MTF of FBP for several different acquisition combinations

Figures 3(a), 3(b) and 3(c) show an example of our mean-subtracted analysis of BP, MITS and FBP, respectively, with seven different combinations of acquisition parameters.

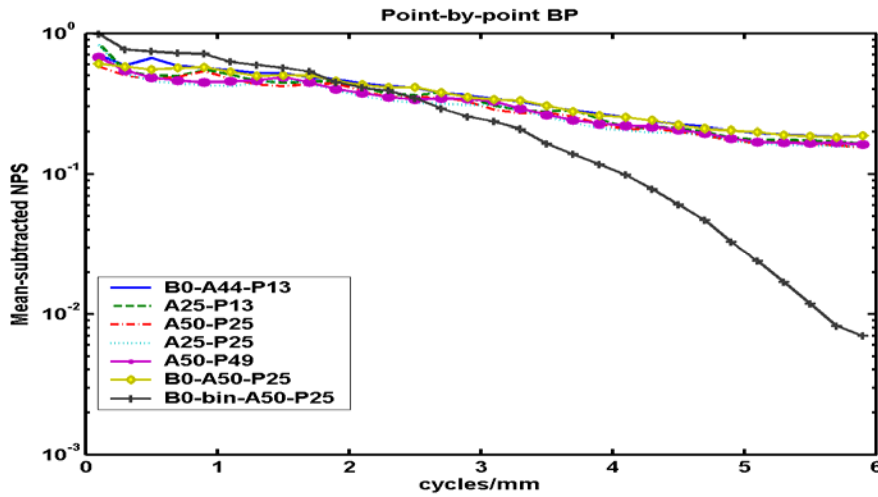


Figure 3(a): Mean-subtracted NPS of BP for several different acquisition combinations

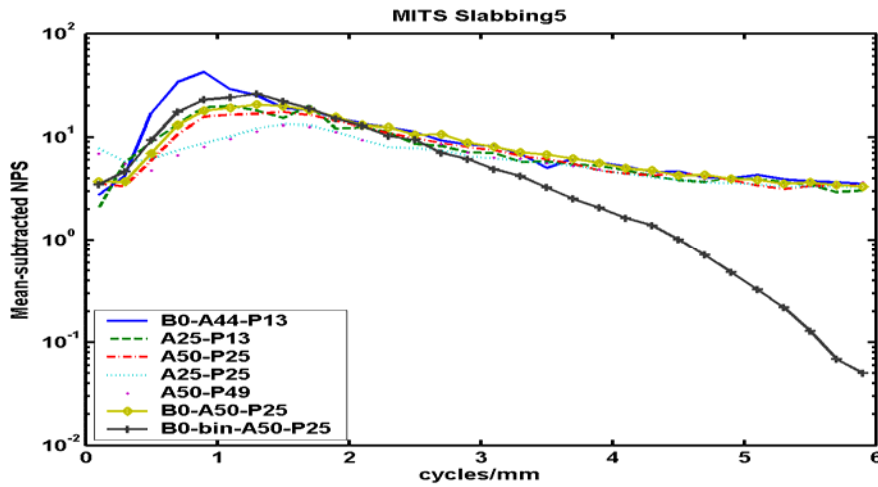


Figure 3(b): Mean-subtracted NPS of MITS for several different acquisition combinations

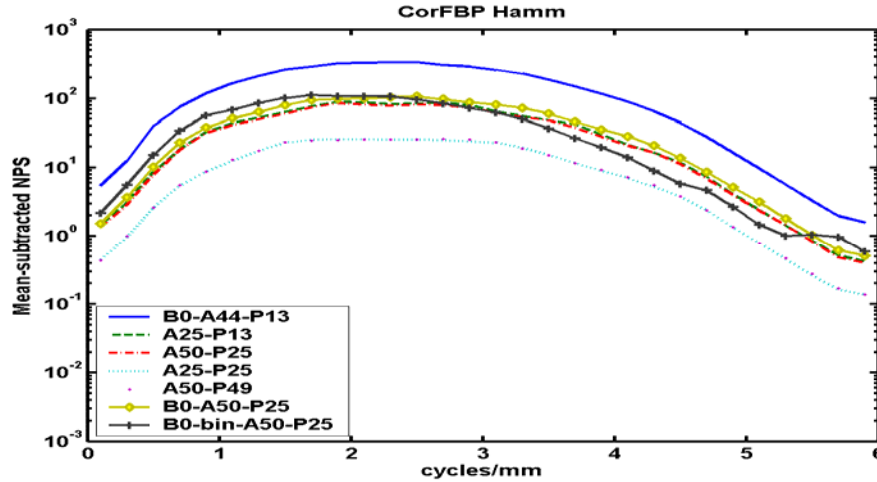


Figure 3(c): Mean-subtracted NPS of FBP for several different acquisition combinations

We found that compared with other acquisition modes, the B0-bin-A50-P25 ($N=25$, $TA=\pm 25^\circ$ angular range, binning mode) has lower high frequency noise characteristics for BP and MITS. Among the other six non-binning acquisition modes, BP performed slightly worse for $N=13$ cases. MITS performed worse for less number of projection images and wider tomographic angle of $N=13$, $TA=\pm 22.5^\circ$ case; MITS had better noise characteristics for bigger number of projection images and wider tomographic angle of $N=49$, $TA=\pm 25^\circ$ case. With same acquisition parameters, the SAA and FBP showed no difference when we varied the RSS. For MITS reconstruction, compared with 2mm and 4mm slice spacing, 1mm slice spacing has better noise response at low-to-middle frequency range. At middle to high frequency range, their noise responses were similar.

We have proposed an image reconstruction algorithm of Gaussian Frequency Blending (GFB) algorithm using NPS analysis to combine MITS and FBT together for better image reconstruction of breast tomosynthesis. We are working on a *Medical Physics* journal manuscript preparation for GFB algorithm.

We have used impulse response and MTF analysis method to compare BP and traditional SAA algorithms (see Appendix #1, #2, and #3). Our results of impulse response analysis for BP with relevance to morphology of structures such as microcalcifications were published in *Medical Physics*, the premiere peer-reviewed journal in the field of Medical Physics, please see Appendix #1 for the reprinted publication.

Task 2. Comparison of different candidate tomosynthesis reconstruction methods (Months 13-24):

To allow for computational modeling, human observer study efforts were scheduled for the second budget year. However, we are relinquishing seven months of the second year because the predoctoral fellowship recipient, Ying Chen, has just received her PhD and graduated.

Instead, we have published a methodology of relative NEQ(f) analysis to compare the efficacy of different candidate tomosynthesis reconstruction methods and have completed the comparison tasks. The methodology of NEQ(f) analysis was published as a proceedings paper at SPIE (see Appendix #4). It combines MTF of signal performance and NPS of noise characteristics to

enable one to evaluate the performance of different acquisition parameters and algorithms for comparison and optimization purposes. For each acquisition parameter and candidate reconstruction algorithm, the same inputs were used in all cases (the same simulated impulse magnitude for relative reconstruction MTF measurement and same accumulative tomosynthesis sequence exposure level for NPS measurement). Therefore, one can make relative comparisons to evaluate performance of different algorithms and acquisition modes with the same inputs. Figures 4(a), 4(b) and 4(c) show an example of our relative NEQ(f) analysis of BP, MITS and FBP respectively with seven different combinations of acquisition parameters.

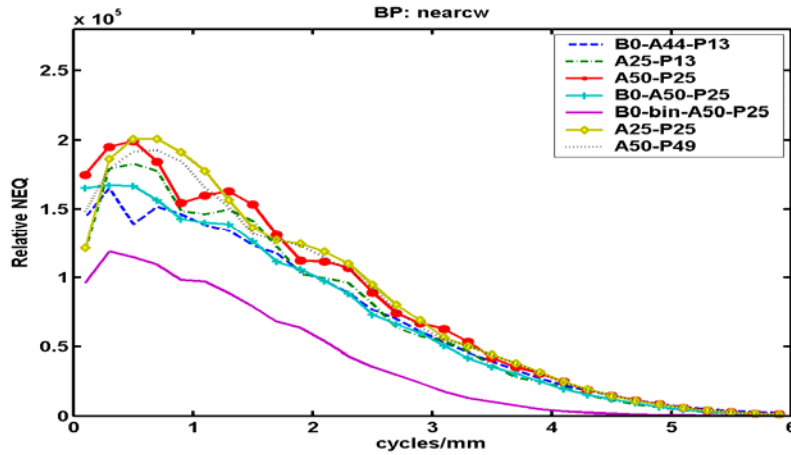


Figure 4(a): Relative NEQ(f) of BP for several different acquisition combinations

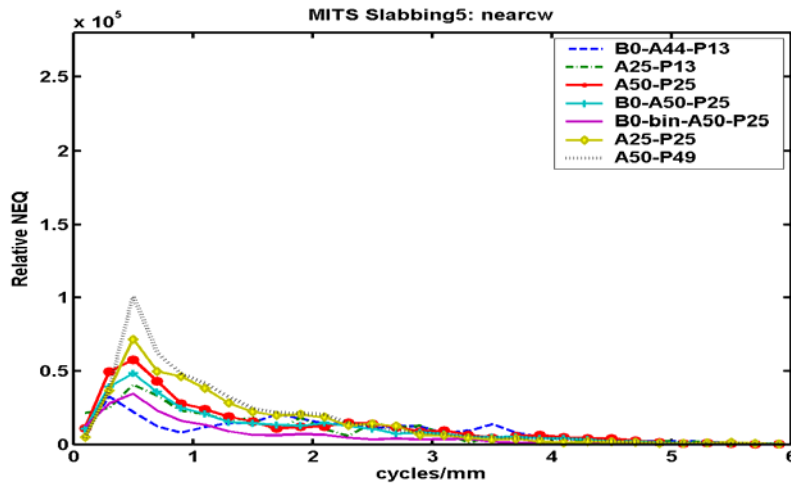


Figure 4(b): Relative NEQ(f) of MITS for several different acquisition combinations

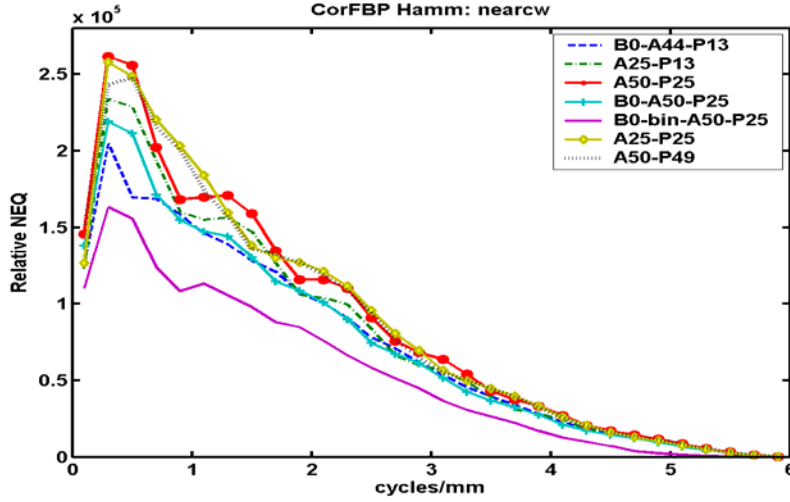


Figure 4(c): Relative NEQ(f) of FBP for several different acquisition combinations

We found that FBP showed better relative NEQ(f) results than that of MITS for the cases investigated. A reason is that MITS was applied on traditional SAA that lines up the structures on the focal plane one-dimensionally; while FBP was applied on point-by-point BP that point-by-point corrects structures on the focal plane. FBP provides a trade-off between wider out-of-plane blur extension and reduced out-of-plane artifacts. FBP with larger number of projection images is the optimal digital breast tomosynthesis image reconstruction method. Considering the longer acquisition time of tomosynthesis sequence of 49 projection images, $N=25$ number of projection images and $TA=50^\circ$ without binning is suggested as the optimal acquisition mode for FBP reconstruction.

The relative NEQ(f) comparison results between MITS and FBP in this project are only limited to breast tomosynthesis imaging. The conclusion doesn't apply to other tomosynthesis applications such as chest imaging where MITS shows advantages in image quality and artifact reduction.

We have published part of our results in a full-length proceedings paper at SPIE (See Appendix #4). We are also working on a *Medical Physics* journal manuscript preparation for our relative NEQ(f) analysis results.

KEY RESEARCH ACCOMPLISHMENTS

- Investigated several different reconstruction algorithms for digital breast tomosynthesis, including SAA, NIKL, BP, MITS, FBP and MLEM. Selected candidate algorithms and compared performance against each candidate algorithm.
- Analyzed impulse response, MTF, and NPS by simulation, experiments and characterization to compare and optimize the imaging acquisition parameters including total Tomographic-Angle (TA), Number of projection images (N), and Reconstruction-Slice-Spacing (RSS).
- Investigated the importance of point-by-point BP for isocentric motion in digital breast tomosynthesis, especially for reconstruction of small structures such as microcalcifications.

- Investigated a new image reconstruction algorithm of Gaussian Frequency Blending (GFB) to combine MITS and FBP together for better breast tomosynthesis image reconstruction.
- Investigated a methodology of relative NEQ(f) analysis for comparison and optimization of different imaging parameters and image reconstruction algorithms. Compared different candidate image reconstruction methods by relative NEQ(f) analysis and found the optimal image reconstruction method of FBP with bigger number of projection images and wider tomographic angular range.
- Ying Chen received a PhD in Biomedical Engineering from Duke University.

REPORTABLE OUTCOMES

The following papers and abstract are attached at appendices 1, 2, 3, and 4 with the same numbers. The names of the fellow (Chen) and mentor (Dobbins) are boldfaced for emphasis.

1. **Y. Chen**, J. Y. Lo, and **J. T. Dobbins III**, “Importance of point-by-point back projection (BP) correction for isocentric motion in digital breast tomosynthesis: Relevance to morphology of microcalcifications,” *Med. Phys.* 34(10), 3885-3892 (2007).
2. **Y. Chen**, J. Y. Lo, **J. T. Dobbins III**, “A Comparison between Traditional Shift-and add (SAA) and Point-by-point Back Projection (BP) – Relevance to Morphology of Microcalcifications for Isocentric Motion in Digit Breast Tomosynthesis (DBT),” *Proceedings of IEEE-Bioinformatics & Bioengineering*, 2007.
3. **Y. Chen**, J. Y. Lo, **J. T. Dobbins III**, “Two-dimensional Shift-And-Add Algorithm for Digital Breast Tomosynthesis Reconstruction,” *Med. Phys.* 33 (6), 2001 (2006).
4. **Y. Chen**, J. Y. Lo, N. T. Ranger, E. Samei, **J. T. Dobbins III**, “Methodology of NEQ(f) analysis for optimization and comparison of digital breast tomosynthesis acquisition techniques and reconstruction algorithms,” *Proc. SPIE 6510, 65101-I*, (2007).

CONCLUSIONS

This work presents the comparison and optimization of several different breast tomosynthesis image reconstruction algorithms and imaging acquisition parameters. We have investigated several different reconstruction algorithms including traditional SAA, BP, NIKL, MITS, FBP and MLEM. We have characterized the impulse response, MTF, and NPS by simulation, experiments, and computation to compare and optimize candidate algorithms and different acquisition parameters.

One important research outcome was the comparison and optimization of algorithms and acquisition parameters. We proposed a relative NEQ(f) analysis to combine the signal and noise performance together. The relative NEQ(f) analysis was applied to DBT for the first time. It provides a means for simultaneously compare signal and noise properties. FBP based on point-by-point BP with more projection numbers was founded to be the best overall method with the highest relative NEQ(f) signal to noise properties.

Additionally, we reported the importance of point-by-point BP for isocentric motion in digital breast tomosynthesis. Additionally, the importance of point-by-point back projection (BP) for isocentric motion in DBT was described and investigated. It improves the in-plane sharpness of structures such as microcalcifications, which bear important meaning in clinical tasks for breast

cancer detection. A novel algorithm of Gaussian Frequency Blending (GFB) to blend MITS and FBP together was also investigated for better image reconstruction of the breast.

REFERENCE

- 1 Daniel B. Kopans, "Breast Imaging," 2nd ed, Lippincott Williams and Wilkins, New York (1997).
- 2 Ralph Highnam, Michael Brady, "Mammographic Image Analysis," Kluwer Academic Publishers, Dordrecht, The Netherlands (1999).
- 3 Lawrence W. Bassett, Valerie P. Jackson, Karin L. Fu, Yao S. Fu, "Diagnosis of Diseases of the Breast", 2nd ed, Elsevier Saunders, Philadelphia, Pennsylvania, 2005.
- 4 Loren T. Niklason, et al., "Digital tomosynthesis in breast imaging", Radiology 205: 399-406, 1997.
- 5 Tao Wu, et al., "Tomographic mammography using a limited number of low-dose cone-beam projection images", Med. Phys. 30 (3): 365-380, March 2003.
- 6 Tao Wu, R. H. Moore, E. A. Rafferty, D. B. Kopans, "A comparison of reconstruction algorithms for breast tomosynthesis", Med. Phys. 9: 2636-2647, September 2004.
- 7 S. Suryanarayanan, A. Karellas, S. Vedantham, S. J. Glick, C. J. D'Orsi, S. P. Baker, and R. L. Webber, "Comparison of tomosynthesis methods used with digital mammography," Acad. Radiol. 7, 1085-1097 (2000).
- 8 S. Suryanarayanan, A. Karellas, S. Vedantham, S. P. Baker, S. J. Glick, C. J. D'Orsi, S. P. Baker, and R. L. Webber, "Evaluation of linear and nonlinear tomosynthetic reconstruction methods in digital mammography," Acad. Radiol. 8, 219-224 (2001).
- 9 L. Zhou, J. Oldan, P. Fisher, and G. Gindi, "Low-contrast lesion detection in tomosynthetic breast imaging using a realistic breast phantom," Proc. SPIE 6142, 1685-1696 (2006).
- 10 Y. Zhang, H. Chan, B. Sahiner, J. Wei, M. M. Goodsitt, L. M. Hadjiiski, J. Ge, C. Zhou, "A comparative study of limited-angle cone-beam reconstruction methods for breast tomosynthesis," Med. Phys. 33(10), 3781-3795 (2006).
- 11 J. T. Rakowski and M. J. Dennis, "A comparison of reconstruction algorithms for C-arm mammography tomosynthesis," Med. Phys. 33(8), 3018-3032 (2006).
- 12 T. Mertelemeier, J. Orman, W. Haerer, and M. K. Dudam, "Optimizing filtered backprojection reconstruction for a breast tomosynthesis prototype device," Proc. SPIE 6142, 131-142 (2006).
- 13 G. M. Stevens, R. Fahrig and N. J. Pelc, "Filtered backprojection for modifying the impulse response of circular tomosynthesis," Med. Phys. 28, 372-380 (2001).
- 14 G. Lauritsch and W. Haerer, "A theoretical framework for filtered back-projection in tomosynthesis," Proc. SPIE 3338, 1127-1137 (1998).
- 15 H. Matsuo, A. Iwata, I. Horiba, and N. Suzumura, "Three-dimensional image reconstruction by digital tomo-synthesis using inverse filtering," IEEE Trans. Med. Imaging 12, 307-313 (1993).
- 16 Y. Chen, J. Y. Lo, J. T. Dobbins III, "Impulse response analysis for several digital tomosynthesis mammography reconstruction algorithms," Proc. SPIE 5745, 541-549 (2005).
- 17 Y. Chen, J. Lo, J. T. Dobbins III, "Matrix Inversion Tomosynthesis (MITS) of the Breast: Preliminary Results," in *RSNA 90th Scientific Assembly*, Chicago, IL, 2004.

- 18 Dobbins, III., "Matrix Inversion Tomosynthesis improvements in longitudinal x-ray slice imaging", U.S. Patent #4,903,204 (1990). Assignee: Duke University.
- 19 Y. Chen, J. Y. Lo, J. A. Baker, J. T. Dobbins III, "Gaussian frequency blending algorithm with Matrix Inversion Tomosynthesis (MITS) and Filtered Back Projection (FBP) for better digital breast tomosynthesis reconstruction," *Proc. SPIE* 6142, 122-130 (2006).
- 20 R. S. Saunders, E. Samei, J. Jesneck, J. Lo, "Physical characterization of a prototype selenium-based full field digital mammography detector," *Med. Phys.* 32(2), 588-599 (2005).
- 21 R. S. Saunders and E. Samei, "A method for modifying the image quality parameters of digital radiographic images," *Med. Phys.* 30, 3006-3017 (2003).
- 22 J. T. Dobbins III, D.L. Ergun, L. Rutz, D. A. Hinshaw, H. Blume, D. c. Clark, "DQE (f) of four generations of computed radiography acquisition devices", *Med. Phys.* 22 (10): 1581-1593 (1995).
- 23 J. T. Dobbins III, "Image quality metrics for digital systems," *Handbook of medical imaging*, Volume1. Physics and Psychophysics, edited by J. Beutel, H. L. Kundel, and R. L. Van Metter. SPIE 1: Ch.3. (2000)

APPENDICES

Four publications and abstract are attached; see "Reportable Outcomes" above for the list.

Importance of point-by-point back projection correction for isocentric motion in digital breast tomosynthesis: Relevance to morphology of structures such as microcalcifications

Ying Chen

Department of Biomedical Engineering, Duke Advanced Imaging Laboratories, Duke University, Durham, North Carolina 27710 and Department of Electrical and Computer Engineering, Southern Illinois University, Carbondale, Illinois 62901

Joseph Y. Lo and James T. Dobbins III

Departments of Radiology and Biomedical Engineering, Duke Advanced Imaging Laboratories, Medical Physics Graduate Program, Duke University, Durham, North Carolina 27710

(Received 27 July 2006; revised 18 June 2007; accepted for publication 31 July 2007; published 19 September 2007)

Digital breast tomosynthesis is a three-dimensional imaging technique that provides an arbitrary set of reconstruction planes in the breast from a limited-angle series of projection images acquired while the x-ray tube moves. Traditional shift-and-add (SAA) tomosynthesis reconstruction is a common mathematical method to line up each projection image based on its shifting amount to generate reconstruction slices. With parallel-path geometry of tube motion, the path of the tube lies in a plane parallel to the plane of the detector. The traditional SAA algorithm gives shift amounts for each projection image calculated only along the direction of x-ray tube movement. However, with the partial isocentric motion of the x-ray tube in breast tomosynthesis, small objects such as microcalcifications appear blurred (for instance, about 1–4 pixels in blur for a microcalcification in a human breast) in traditional SAA images in the direction perpendicular to the direction of tube motion. Some digital breast tomosynthesis algorithms reported in the literature utilize a traditional one-dimensional SAA method that is not wholly suitable for isocentric motion. In this paper, a point-by-point back projection (BP) method is described and compared with traditional SAA for the important clinical task of evaluating morphology of small objects such as microcalcifications. Impulse responses at different three-dimensional locations with five different combinations of imaging acquisition parameters were investigated. Reconstruction images of microcalcifications in a human subject were also evaluated. Results showed that with traditional SAA and 45° view angle of tube movement with respect to the detector, at the same height above the detector, the in-plane blur artifacts were obvious for objects farther away from x-ray source. In a human subject, the appearance of calcifications was blurred in the direction orthogonal to the tube motion with traditional SAA. With point-by-point BP, the appearance of calcifications was sharper. The point-by-point BP method demonstrated improved rendition of microcalcifications in the direction perpendicular to the tube motion direction. With wide angles or for imaging of larger breasts, this point-by-point BP rather than the traditional SAA should also be considered as the basis of further deblurring algorithms that work in conjunction with the BP method. © 2007 American Association of Physicists in Medicine. [DOI: [10.1118/1.2776256](https://doi.org/10.1118/1.2776256)]

Key words: mammography, tomosynthesis, 3D reconstruction, shift-and-add (SAA), back projection, microcalcifications

I. INTRODUCTION

Breast cancer is the most common cancer among women. Currently, mammography is the most important and efficacious tool for the early detection of breast cancer.¹ However, limitations of mammography have been well publicized, such as 20% false negative rate,^{2,3} many callbacks from screening, and low positive predictive value of about 15%–34% from biopsy.^{4,5} It can be difficult for conventional two-dimensional (2-D) mammography to distinguish a cancer from overlying breast tissues.

Digital breast tomosynthesis is a three-dimensional (3-D) imaging technique that provides an arbitrary set of recon-

struction planes in the breast from a limited-angle series of projection images when the x-ray tube moves.⁶ There are a variety of tomosynthesis reconstruction algorithms, including the image-stretching method proposed by Niklason and colleagues,⁷ maximum likelihood iterative algorithm by Wu *et al.*,⁸ tuned-aperture computed tomography (TACT) reconstruction methods developed by Webber and investigated by Suryanarayanan *et al.*,^{9,10} algebraic reconstruction techniques,^{11–13} filtered back projection (FBP),^{14–20} matrix inversion tomosynthesis (MITS),^{17,21–24} and Gaussian frequency blending of MITS and FBP.¹⁵ Some of these algorithms depend on a traditional shift-and-add (SAA) method that is appropriate for parallel-path geometries. For example,

Niklason and colleagues modified the traditional shift-and-add technique for mammography to stretch the image along the direction of x-ray tube motion to account for the effects of magnification variation with angle, but the correction necessary along the direction perpendicular to the tube motion was not taken into account.⁷ Suryanarayanan *et al.* applied Webber's TACT method to breast tomosynthesis reconstruction,^{9,10} and used traditional SAA. The MITS technique developed in our laboratory has been investigated for breast tomosynthesis using a traditional SAA algorithm as the basis for subsequent matrix inversion deblurring.²¹

Traditional SAA is appropriate for parallel-path tube movement when the path of the tube lies in a plane parallel to the plane of the detector.⁶ However, the partial isocentric motion of the tube in breast tomosynthesis causes a non-parallel motion. The path of the tube does not lie in a plane that is parallel to the detector plane. While the effects due to isocentric motion are small for most objects, the use of SAA methods introduces morphological distortions with small objects such as microcalcifications. Therefore, a simple SAA reconstruction algorithm is not entirely suitable for breast tomosynthesis. This issue of non-parallel motion is addressed in point-by-point back projection (BP) methodologies,¹⁴ but its impact has largely not been evaluated with algorithms that rely simply on traditional SAA approaches. This paper demonstrates the importance of point-by-point corrections for isocentric motion in digital breast tomosynthesis by examining how the morphology of microcalcification reconstructions changes relative to a traditional SAA method that does not employ point-by-point corrections.

In this paper, a point-by-point BP correction method is described and compared with traditional SAA by analysis of impulse response. Impulse responses at different 3-D locations with five different combinations of imaging acquisition parameters were investigated. In addition, reconstructed images of a calcification in a human subject were evaluated to demonstrate the improvement in the morphology of microcalcifications associated with the point-by-point BP correction method.

II. METHODS

II.A. Breast tomosynthesis system

A selenium-based direct conversion Siemens Mammomat Novation DR prototype system was modified to be used as the breast tomosynthesis acquisition system.²⁵ The detector area was 24 cm × 30 cm (2816 × 3584 pixels), with a pixel pitch of 85 μm (different from that used in the clinical digital mammography system from the same manufacturer). Several different modes were provided to choose from different available projection numbers, total angular range and speeds with exposure and readout cycle between 0.5 and 0.8 seconds per image. Figure 1 shows a diagram of the breast tomosynthesis imaging system. During the tomosynthesis procedure, the x-ray tube moves automatically along an arc above the chest wall to acquire up to 49 projection images. A continuous x-ray motion was employed. The distance R from the rotation center O to the detector is 6 cm. The range of the

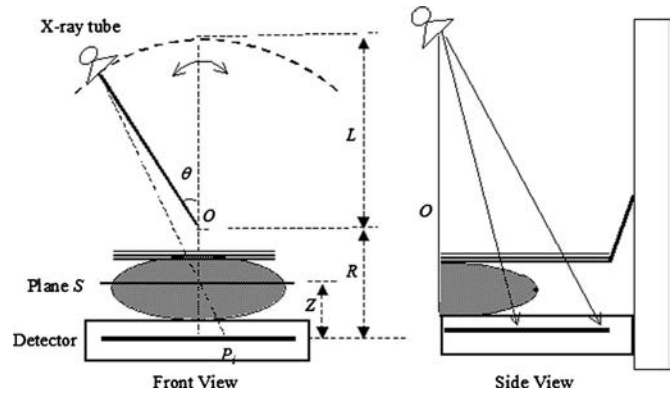


FIG. 1. Breast tomosynthesis imaging system. O is the rotation center, R is the rotation center to detector distance, L is the rotation arm length, and Z is the height of plane S above the detector.

actual view angles can be up to about 45° with respect to the detector (50° at the rotation center). A compression paddle is used to keep the object still.

II.B. Traditional shift-and-add algorithm

The traditional SAA tomosynthesis reconstruction algorithm^{6,17} is a common mathematical method to line up each projection image based on its relative shift to generate reconstruction slices at specified depths. When the x-ray tube moves, objects at different heights above the detector will be projected onto the detector at positions depending on the relative heights of the objects.

In order to reconstruct slice images of the breast, each projection image should be shifted by an amount appropriate for the plane of reconstruction. If the detector remains stationary and the tube moves in a plane that is parallel to the detector plane, the magnification of objects depends only on the height of the object. With the traditional SAA algorithm for breast tomosynthesis reconstruction, shift amounts for each projection plane are calculated along the axis of x-ray tube movement. In this paper, the shift amount was calculated based on projected positions from central points of each reconstruction plane. The shifted planes were added together to emphasize structures in the in-focus plane and blur out structures in other planes.

As shown in Fig. 1, plane S represents a reconstruction plane at a height of Z above the detector surface. When the x-ray tube moves, objects in plane S will be projected onto the detector surface. For a specific projection image from angle θ , in order to shift the projection image to line up structures from plane S , the traditional SAA algorithm uses the shift amount calculated as

$$\text{shift}_i(Z) = P_i(Z) = L \sin \theta \frac{Z}{L \cos \theta + (R - Z)}, \quad (1)$$

where L is length of the rotation arm, and R is the height of the rotation axis from the detector surface. One can obtain the reconstruction plane S as the average of all N shifted projection images:

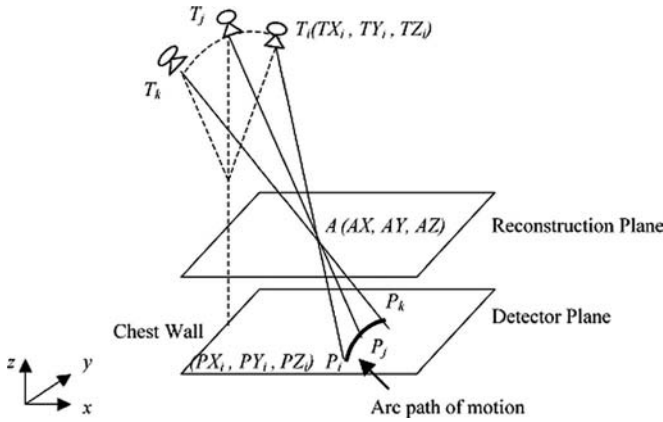


FIG. 2. Two-dimensional arc path from isocentric tube motion.

$$T(x, y) = \frac{1}{N} \sum_{i=1}^N I_i(x, y) \otimes \delta[y - \text{shift}_i(Z)]. \quad (2)$$

II.C. Point-by-point back projection algorithm

With parallel tube motion, the traditional SAA method works well as long as the required shifting is the same for all pixels in the reconstruction plane. However, because of the isocentric motion of the x-ray tube, a shift actually occurs in both x and y directions on each projection image, and the shifting amount is not uniform for all pixels on the reconstruction plane. Figure 2 shows the arc path of motion when the x-ray tube moves along the Y axis. Point A represents a single structure on a certain reconstruction plane. P_i , P_j , and P_k are the actual projected locations of point A on the detector with different x-ray tube locations of T_i , T_j , and T_k . The actual path of projected locations follows a 2-D arc rather than a one-dimensional line. Therefore, to reconstruct a single pixel on a reconstruction plane at certain height above the detector, the shift amount should be considered along both x and y directions for every pixel on the reconstruction plane.

With the point-by-point BP algorithm, shift amounts for every pixel location on each reconstructed plane were computed, taking into account the 2-D arc projection location of reconstructed objects in each plane. In Fig. 2, (Ax, Ay, Az) represent coordinates of point A . (Tx_i, Ty_i, Tz_i) represents the tube position along the x , y , z axes when the tube moves to position T_i . (Px_i, Py_i, Pz_i) represents projected coordinates of points A on the projection image. One can calculate the two-dimensional shift amount as

$$Px_i = Tx_i - \frac{(Tx_i - Ax)(Tz_i - Pz_i)}{Tz_i - Az}, \quad (3)$$

$$Py_i = Ty_i - \frac{(Ty_i - Ay)(Tz_i - Pz_i)}{Tz_i - Az}.$$

Since P_i is located on the detector, one can define $Pz_i = 0$. Thus, the above formula can be simplified as

$$Px_i = Tx_i + \frac{(Tx_i - Ax)Tz_i}{Tz_i - Az}, \quad (4)$$

$$Py_i = Ty_i + \frac{(Ty_i - Ay)Tz_i}{Tz_i - Az}. \quad (4)$$

The final pixel value of point A in the tomosynthesized reconstruction was calculated as $(1/N) \sum_{i=1}^N I(P_i)$ where $I(P_i)$ is the pixel value at a given location on the i th projection image, and N is the total number of projection images. In this paper, bilinear interpolation was used to address the issue of partial pixel locations. Computation times for the point-by-point BP algorithm are roughly comparable to the SAA method. With a computer of 800 MHz CPU and UNIX operating system, it takes less than 5 min for either the point-by-point BP or traditional SAA reconstruction.

II.D. Impulse response analysis

A single delta function was simulated by ray-tracing method as the input impulse to investigate the sharpness of reconstructed in-plane structures and to see how the traditional SAA and point-by-point BP algorithm differ from each other. Two different impulse locations were investigated in this paper: (1) an impulse that is near the chest wall (20 pixels away from the chest wall) and in a defined reconstructed plane (40 mm above the detector surface); and (2) an impulse that is approximately 4 cm away from the chest wall and in a defined reconstructed plane (40 mm above the detector surface). Parameters of the digital breast tomosynthesis device described in Sec. II A were used for geometries of the simulation. Five different combinations of acquisition parameters including projection image numbers and total angular range were applied: (1) 13 projections with 22.7° view angle range with respect to the detector; (2) 13 projections with 45° view angle range with respect to the detector; (3) 25 projections with 22.7° view angle range; (4) 25 projections with 45° view angle range with respect to the detector; and (5) 49 projections with 45° view angle range. For each impulse location and combination of acquisition parameters, two datasets of projection images were simulated by ray-tracing method: (1) background-only: only I/r^2 shading difference for each pixel on projection images was taken into account (r is the distance from the x-ray source to each pixel location); and (2) impulse-added: projection images with simulated impulse and the I/r^2 shading difference. Other system blur and noise issues are not addressed in this paper in order to focus on the contribution of the blur due to the isocentric motion. During ray-tracing, if the simulated impulse was projected onto non-integer pixel location on the detector surface, linear interpolation of the projected impulse among four neighboring pixels was performed.

Traditional SAA and point-by-point BP reconstruction algorithms were applied to both impulse-added and background-only simulated tomosynthesis projection sequences. A reconstruction plane spacing of 1 mm was used.

Reconstruction images from background-only projections were subtracted from reconstructions of impulse-added projections to eliminate background shading effects. Because of the isocentric motion, there will be greater interpolation that will affect the amplitude of the impulse response further away from the chest wall. In order to compare impulse responses at different locations, the impulse responses were normalized based on the ideal condition when the impulse is exactly located underneath the x-ray source. Under this ideal condition, the impulse was only projected along the tube's motion direction and no interpolation was involved in the direction orthogonal to the tube's motion direction.

II.E. Human subject images

Human subject images have been acquired on our prototype breast tomosynthesis system under an IRB-approved protocol. Images of one human subject with notable calcifications were reconstructed with the traditional SAA and point-by-point BP methods to demonstrate the effect of the point-by-point BP method on reconstructed calcification morphological appearance. A tomosynthesis sequence was acquired with 25 projection images and a total view angle of 45° with respect to the detector (50° at the rotation center). The radiographic technique for breast tomosynthesis was selected using technique optimization procedures reported previously.²⁶ The target/filter for tomosynthesis exams is tungsten/rhodium. The kilovoltage setting is selected to maximize a figure of merit (signal difference to noise ratio squared per unit dose) for a given breast thickness and density. Then the mAs can be chosen to compare the dose levels required to achieve the same image quality when compared against the conventional molybdenum/molybdenum or molybdenum/rhodium technique, or alternatively to compare the image quality for the same dose level. For this specific subject, we chose to do the latter. By using the tomosynthesis technique of W/Rh at 28 kVp (half-value layer 0.50 mm Al) and 112 mAs for this 100% fatty, 45 mm breast, we maintained the same dose as the conventional left cranio caudal mammogram.

III. RESULTS

III.A. Impulse responses

Figures 3–5 show the impulse response results with a simulated impulse located in a defined reconstruction plane at 40 mm above the detector, and approximately 4 cm away from the chest wall. Figure 3 shows results from simulated acquisition parameters of 25 projections and 45° view angle range with respect to the detector. Figure 4 shows results from 13 projections and 45° view angle range with respect to the detector. Figures 5 shows results from 25 projections and a narrower view angle range of 22.7° with respect to the detector. On Figs. 3 through 5, (a) and (c), give corresponding values in a plane at the exact height of the impulse's location; (b) and (d) give the impulse response of reconstruction planes 1 mm lower than the impulse's location; (a) and (b) are results from point-by-point BP; and (c) and (d) are

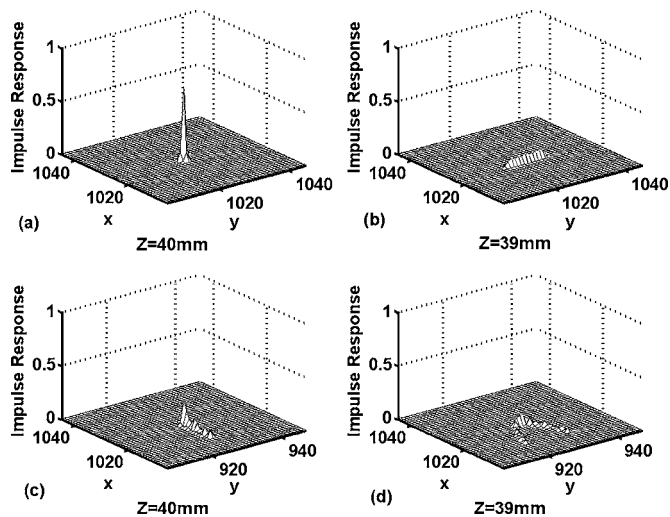


FIG. 3. Traditional SAA and point-by-point BP impulse responses: 25 projection images and 45° view angle range with respect to the detector, with the impulse located 40 mm above the detector and about 4 cm away from the chest wall. (a) and (b) give the impulse response of point-by-point BP; (c) and (d) give the impulse response of traditional SAA. (a) and (c) are impulse responses in the plane at the exact height of the impulse's location; (b) and (d) give corresponding values in a reconstruction plane 1 mm below the impulse's location.

results from traditional SAA. The x and y axes give the pixel location on the reconstruction plane, and the plot displays the normalized amplitude of the response. The X axis represents the direction orthogonal to the tube's motion direction. The Y axis represents the tube's motion direction. Only a 40×40 pixel region close to the impulse is shown for clarity.

One can see that with traditional SAA, when the impulse is 4 cm away from the chest wall and the x-ray source moves

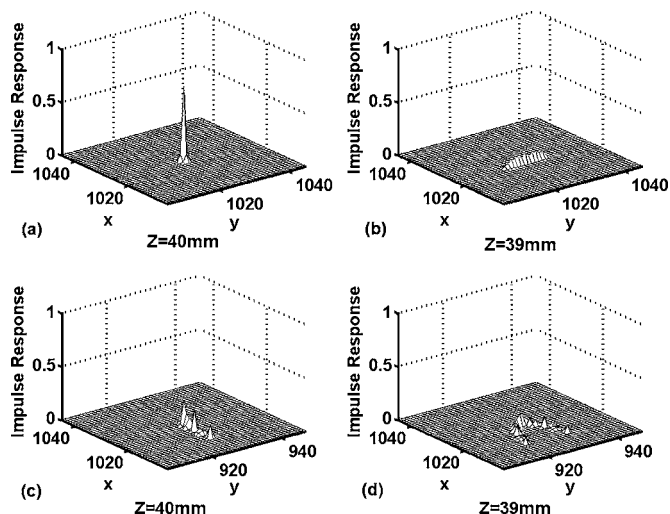


FIG. 4. Traditional SAA and point-by-point BP impulse responses: 13 projection images and 45° view angle range with respect to the detector, with the impulse located 40 mm above the detector and about 4 cm away from the chest wall. (a) and (b) give the impulse response of point-by-point BP; (c) and (d) give the impulse response of traditional SAA. (a) and (c) are impulse responses in the plane at the exact height of the impulse's location; (b) and (d) give corresponding values in a reconstruction plane 1 mm below the impulse's location.

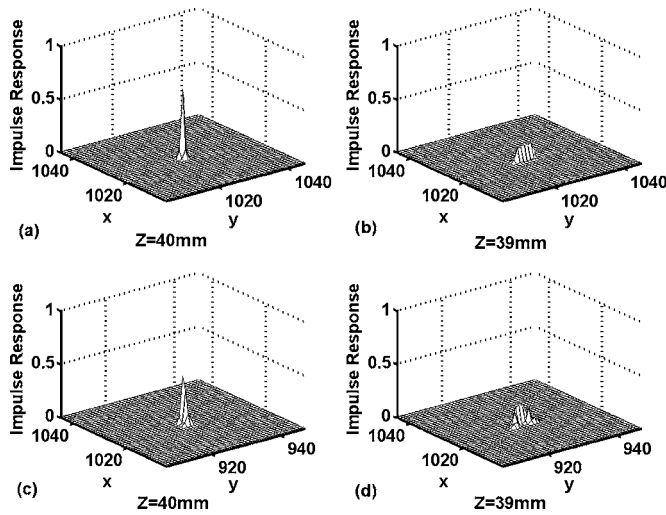


FIG. 5. Traditional SAA and point-by-point BP impulse responses: 25 projection images and 22.7° view angle range with respect to the detector, with the impulse located 40 mm above the detector and about 4 cm away from the chest wall. (a) and (b) give the impulse response of point-by-point BP; (c) and (d) give the impulse response of traditional SAA. (a) and (c) are impulse responses in the plane at the exact height of the impulse's location; (b) and (d) give corresponding values in a reconstruction plane 1 mm below the impulse's location.

along a wider view angle range of 45° , the in-plane response is noticeably blurred and multiple peaks exist in a direction that is perpendicular to the direction of tube movement [Figs. 3(c) and 4(c)], reflecting the uncorrected partial isocentric tube motion. With point-by-point BP, the in-plane response is much sharper [Figs. 3(a) and 4(a)]. When the number of projection images decreases to 13, the in-plane response and out-of-plane blur become discrete [Figs. 4(b) and 4(d)] due to limited projection numbers. With a narrower view angle range of 22.7° , the differences between traditional SAA and point-by-point BP are less obvious (Fig. 5). However, one can still say that the in-plane response of point-by-point BP is higher and sharper than that of traditional SAA.

Table I gives the full width at half-maximum (FWHM) measurement and full width at a tenth-maximum values (FWTM) of the in-plane impulse responses along two orthogonal directions when the impulse is located at 40 mm

above the detector surface and near chest wall. Table II gives the same measurements of FWHM and FWTM when the impulse is located 4 cm away chest wall. When the impulse is located near the chest wall, there is only a small difference (<1 pixel size) in FWHM and FWTM values between traditional SAA and point-by-point BP for each combination of acquisition parameters. With a narrower view angle range of 22.7° , differences are small too (less than 1 pixel size). However, with a wider view angle range of 45° , when the impulse is located 4 cm away the chest wall, major differences exist along the X axis (direction orthogonal to tube's motion direction). Multiple peaks and blurs appear along this direction [Figs. 3(c) and 4(c)]. Due to multiple peaks along the X axis, FWHM cannot adequately represent the real extension of impulse response; for that reason, the measurement of FWTM was also provided. The difference in FWTM values is as large as 9 pixels between traditional SAA and point-by-point BP. The blur associated with tomosynthesis approaches was estimated by the modulation transfer function (MTF) measurement of the middle projection (0°) with tube moving.²⁷ The estimated FWHM and FWTM values from blur including motion blur and system blur were 1.2 and 2.2 pixels.

III.B. Human subject images

Figure 6 shows regions of interest containing two calcifications from images of the left (L) breast of the human subject. Reconstructed structures by traditional SAA and point-by-point BP methods are compared. A 12.75×12.75 mm² region-of-interest (ROI) is demonstrated. Compared with traditional SAA, edges of calcifications are sharper and better focused with point-by-point BP [Figs. 6(b) and 6(e)]. A quantitative measurement of the shape and width of the punctate calcification (left-most calcification) on this ROI is given in Table III. The Y axis corresponds to the direction of x-ray tube motion, and the X axis is the direction orthogonal to the tube motion direction. One can see that, compared with the traditional SAA, point-by-point BP provided clearer edge shape and narrower width along X axis that is perpendicular to the x-ray tube motion direction.

TABLE I. The impulse is located near chest wall. Full width at half-maximum and full width at tenth-maximum measurements of in-plane impulse response along two directions: tube's motion direction (Y axis) and direction orthogonal to tube's motion (X axis).

Acquisition parameters		Full width at tenth-maximum (in pixels)				Full width at half-maximum (in pixels)			
Projections	View angle range ($^\circ$)	Traditional SAA		Point-by-point BP		Traditional SSA		Point-by-point BP	
		X axis	Y axis	X axis	Y axis	X axis	Y axis	X axis	Y axis
13	22.7	2.8	2.8	3.4	2.4	1.9	1.2	1.7	1.2
25	22.7	2.8	2.8	3.5	2.4	1.9	1.2	1.6	1.2
13	45	2.7	2.7	3.1	2.1	1.4	1.2	1.3	1.2
25	45	2.7	2.8	3.2	2.3	1.4	1.2	1.4	1.2
49	45	2.7	2.6	3.2	2.1	1.5	1.2	1.4	1.2

TABLE II. The impulse is located 4 cm away chest wall. Full width at half-maximum and full width at tenth-maximum measurements of in-plane impulse response along two directions: tube's motion direction (Y axis) and direction orthogonal to tube's motion (X axis).

Acquisition Parameters		Full Width at Tenth Maximum (in pixels)				Full Width at Half Maximum (in pixels)			
Projections	View angle range ($^{\circ}$)	Traditional SAA		Point-by-point BP		Traditional SSA		Point-by-point BP	
		X axis	Y axis	X axis	Y axis	X axis	Y axis	X axis	Y axis
13	22.7	3.7	2.8	2.8	2.5	2.0	1.2	1.2	1.2
25	22.7	3.6	2.8	2.6	2.3	2.0	1.2	1.2	1.2
13	45	11.8	2.5	2.2	2.1	(~ 13) ^a	1.2	1.2	1.2
						Multiple peaks			
25	45	11.7	2.8	2.4	2.4	(~ 13) ^a	1.2	1.2	1.2
						Multiple peaks			
49	45	11.4	2.8	2.6	2.1	(~ 13) ^a	1.2	1.2	1.2
						Multiple peaks			

^aFor the 45° scan, multiple discrete peaks in the impulse response make FWHM not meaningful as a descriptor of impulse width. For these cases, the approximate overall width of the impulse is provided.

Figure 7(a) is a low dose middle projection image of the same human breast when the x-ray tube was positioned at the 0° position. Figures 7(b) and 7(c) are reconstructed slice images by traditional one-dimensional SAA and point-by-point BP, respectively, at a height of 7.5 mm above the detector. The reconstructed size of the breast by traditional one-dimensional SAA is larger than that from point-by-point BP [Figs. 7(b) and 7(c)]. This is due to the uncorrected magnification difference with traditional SAA for structures at different locations in the reconstruction plane. When the structures are located at difference heights above the detector surface, differences in magnification exist. Structures at higher locations above the detector surface will be projected onto the detector with a larger size. Traditional SAA does not

take this magnification difference into account. After shift-and-add, structures at higher locations appear larger compared with the same size structure at lower location. The reconstructed structure size from traditional SAA reconstruction cannot reflect the real structure size. Point-by-point BP correctly addressed this magnification difference issue by calculating shift amounts for every pixel location on each reconstruction plane. Therefore, the point-by-point BP reconstructed plane in Fig. 7(c) reflects the real size and is smaller than that from traditional SAA.

IV. DISCUSSION

With the traditional SAA algorithm for digital breast tomosynthesis reconstruction, shift amounts for each projection plane are calculated along the direction of the x-ray tube's movement. However, due to the isocentric motion of x-ray tube, shift amounts are not the same for all pixels on a reconstruction plane at certain height above the detector. The track of projected impulse locations actually occurs in two dimensions on the detector. Different shift amount is required by different pixel location on a reconstruction plane. As a result, the in-plane structures are blurred. Illustrations with impulse responses and reconstructed human subject images demonstrated that this is an inherent problem of traditional one-dimensional SAA with breast tomosynthesis. This problem is more obvious when the object is farther away from the chest wall and higher above the detector. Thus, with traditional SAA, objects such as microcalcifications appear blurred and their apparent morphology changes.²⁸

With point-by-point BP, the artifacts coming from the isocentric x-ray tube's movement are corrected. The in-plane structures are sharper. While reconstructions of gross anatomy were adequate with either algorithm, the morphology of small structures such as microcalcifications reconstruction requires a point-by-point correction. Morphological

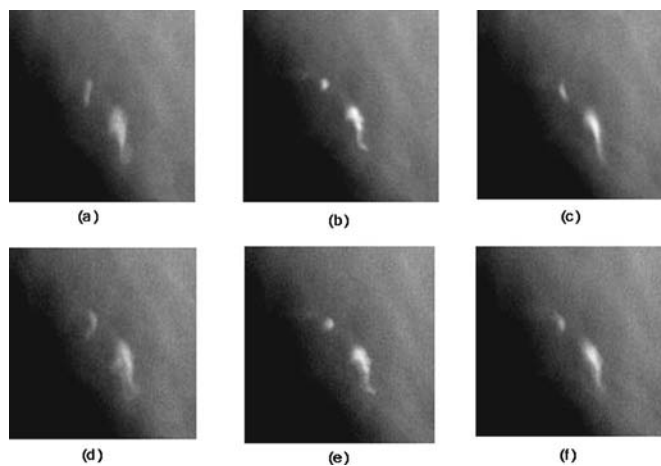


FIG. 6. Reconstructed 12.75×12.75 mm² ROI of a human breast containing calcifications, $Z=18$ mm represents the plane height closest to the location of the calcification: (a) point-by-point BP, $Z=16.5$ mm; (b) point-by-point BP, $Z=18$ mm; (c) point-by-point BP, $Z=19.5$ mm; (d) traditional SAA, $Z=16.5$ mm; (e) traditional SAA, $Z=18$ mm; (f) traditional SAA, $Z=19.5$ mm.

TABLE III. Quantitative measurement of the leftmost calcification depicted in Fig. 6. Estimated accuracy of measurement is ± 1 pixel.

Z=16.5 mm				Z=18 mm			Z=19.5 mm		
Shape		Width (in pixels)		Shape	Width (in pixels)		Shape	Width (in pixels)	
		X	Y		X	Y		X	Y
Traditional SAA	Curvilinear	10	21	Punctate blurred	9	11	Indistinct	11	16
Point-by-point BP	linear	7	20	Punctate sharp	7	9	Curvilinear	7	17

artifacts were reduced with the point-by-point correction, and rendition of small objects such as microcalcifications were greatly improved. These results demonstrate the importance of using a point-by-point correction to remove isocentric motion artifacts in tomosynthesis imaging of the breast, where the morphology of microcalcifications has an important bearing on clinical decision making.

The source of the difficulties with traditional SAA is the variable magnification introduced by the partial isocentric motion of the x-ray tube. The magnification of objects in different reconstruction slices varies from plane-to-plane as a function of the height of slices above the detector. Even within the same reconstruction plane, the magnification also changes at different pixel locations due to the partial isocentric motion. Traditional SAA does not take this issue into account. With point-by-point BP, the shift amount is calculated according to the exact location of the pixel in the reconstruction slices, thereby addressing this issue of variable magnification.

None of methods commonly used for breast tomosynthesis is truly spatially invariant due to the partial isocentric

tube motion, although for structures close to the chest wall and near the detector, the imaging system is approximately spatially invariant. Therefore, linear deblurring techniques will demonstrate less uniform behavior in breast tomosynthesis geometries than in parallel-path tomosynthesis geometries. We found that when the impulse is located near the chest wall or when the total view angle range is narrower such as 22.7° with respect to the detector, there is no big difference (<1 pixel size) in FWHM and FWTM values between traditional SAA and point-by-point BP for a reconstruction with a height of 40 mm above the detector. However, with a wider view angle range of 45° , even moving the impulse 4 cm away chest wall shows a difference (about 9 pixels) along the direction orthogonal to the direction of tube motion. Therefore, with a narrow angle, or for small or thin breasts, the SAA algorithm may be tolerated. However, with a wide angle or large breast size, the point-by-point BP algorithm rather than traditional SAA should be used to minimize issues related to isocentric motion. Deblurring algorithms such as FBP or MITS, which are an important component of high-quality tomosynthesis reconstruction, should use the point-by-point BP method rather than the SAA method to generate the constituent images prior to deblurring under the same conditions of wide tube angle or large breast size.

V. CONCLUSIONS

This work demonstrates that point-by-point BP is an effective method to reconstruct 3-D tomosynthesis images of the breast with improved rendition of small structures such as microcalcifications. Compared with the traditional SAA algorithm, the method of point-by-point BP takes into account the variable magnification and shift occurring along the direction orthogonal to tube movement due to the isocentric tube motion. Point-by-point BP improves the sharpness and morphology of structures especially for small objects such as calcifications. This may prove helpful to radiologists in discriminating malignant from benign microcalcification patterns, and thereby improve the accuracy of breast cancer detection.

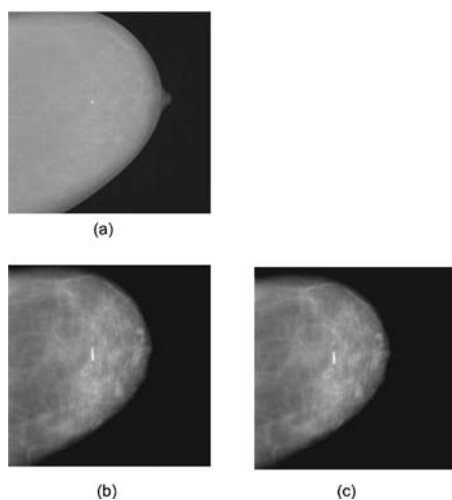


FIG. 7. A human breast demonstrating a solitary calcification: (a) low dose middle (0°) projection image of the tomosynthesis sequence. The spectrum used for the tomosynthesis sequence was 28 kVp with W/Rh target/filter and 112.5 mAs for a total of 25 projection images and 45° view angle range with respect to the detector. (b) Traditional SAA reconstructed slice image: Z=7.5 mm. (c) Point-by-point BP reconstructed slice image: Z=7.5 mm.

ACKNOWLEDGMENTS

We thank Jay A. Baker, M.D., at Duke University Medical Center for clinical insight and helpful discussion. This work was supported by a grant from U.S. Army Medical Research and Materiel Command (USAMRMC W81XWH-06-1-0462), a research grant from Siemens Medical Solutions, and NIH R01 112437.

- ¹L. W. Bassett, V. P. Jackson, K. L. Fu, and Y. S. Fu, *Diagnosis of Diseases of the Breast*, 2nd ed. (Elsevier Saunders, Philadelphia, PA, 2005).
- ²L. J. W. Burhenne, S. A. Wood, C. J. D'Orsi, S. A. Feig, D. B. Kopans, K. F. O'Shaughnessy, E. A. Sickles, L. Tabar, C. J. Vyborny, and R. A. Castellino, "Potential contribution of computer-aided detection to the sensitivity of screening mammography," *Radiology* **215**, 554–562 (2000).
- ³L. H. C. Burrell, D. M. Sibbering, A. R. Wilson, S. E. Pinder, A. J. Evans, L. J. Yeoman, C. W. Elston, I. O. Ellis, R. W. Blamey, and J. F. Tobertson, "Screening interval breast cancers: Mammographic features and prognosis factors," *Radiology* **199**, 811–817 (1996).
- ⁴A. M. Knutzen and J. J. Gisvold, "Likelihood of malignant disease for various categories of mammographically detected, nonpalpable breast lesions," *Mayo Clin. Proc.* **68**, 454–460 (1993).
- ⁵D. B. Kopans, "The positive predictive value of mammography," *AJR, Am. J. Roentgenol.*, **158**, 521–526 (1992).
- ⁶J. T. Dobbins III and D. J. Godfrey, "Digital x-ray tomosynthesis: Current state of the art and clinical potential," *Phys. Med. Biol.* **48**, 65–106 (2003).
- ⁷L. T. Niklason *et al.*, "Digital tomosynthesis in breast imaging," *Radiology* **205**, 399–406 (1997).
- ⁸T. Wu *et al.*, "Tomographic mammography using a limited number of low-dose cone-beam projection images," *Med. Phys.* **30**, 365–380 (2003).
- ⁹S. Suryanarayanan, A. Karellas, S. Vedantham, S. J. Glick, C. J. D'Orsi, S. P. Baker, and R. L. Webber, "Comparison of tomosynthesis methods used with digital mammography," *Acad. Radiol.* **7**, 1085–1097 (2000).
- ¹⁰S. Suryanarayanan, A. Karellas, S. Vedantham, S. P. Baker, S. J. Glick, C. J. D'Orsi, S. P. Baker, and R. L. Webber, "Evaluation of linear and non-linear tomosynthetic reconstruction methods in digital mammography," *Acad. Radiol.* **8**, 219–224 (2001).
- ¹¹L. Zhou, J. Oldan, P. Fisher, and G. Gindi, "Low-contrast lesion detection in tomosynthetic breast imaging using a realistic breast phantom," *Proc. SPIE* **6142**, 1685–1696 (2006).
- ¹²Y. Zhang, H. Chan, B. Sahiner, J. Wei, M. M. Goodsitt, L. M. Hadjiiski, J. Ge, and C. Zhou, "A comparative study of limited-angle cone-beam reconstruction methods for breast tomosynthesis," *Med. Phys.* **33**, 3781–3795 (2006).
- ¹³J. T. Rakowski and M. J. Dennis, "A comparison of reconstruction algorithms for C-arm mammography tomosynthesis," *Med. Phys.* **33**, 3018–3032 (2006).
- ¹⁴T. Wu, R. H. Moore, E. A. Rafferty, and D. B. Kopans, "A comparison of reconstruction algorithms for breast tomosynthesis," *Med. Phys.* **9**, 2636–2647 (2004).
- ¹⁵Y. Chen, J. Y. Lo, J. A. Baker, and J. T. Dobbins III, "Gaussian frequency blending algorithm with matrix inversion tomosynthesis (MITS) and filtered back projection (FBP) for better digital breast tomosynthesis reconstruction," *Proc. SPIE* **6142**, 122–130 (2006).
- ¹⁶T. Mertelemeier, J. Orman, W. Haerer, and M. K. Dudam, "Optimizing filtered backprojection reconstruction for a breast tomosynthesis prototype device," *Proc. SPIE* **6142**, 131–142 (2006).
- ¹⁷Y. Chen, J. Y. Lo, and J. T. Dobbins III, "Impulse response analysis for several digital tomosynthesis mammography reconstruction algorithms," *Proc. SPIE* **5745**, 541–549 (2005).
- ¹⁸G. M. Stevens, R. Fahrig, and N. J. Pelc, "Filtered backprojection for modifying the impulse response of circular tomosynthesis," *Med. Phys.* **28**, 372–380 (2001).
- ¹⁹G. Lauritsch and W. Haerer, "A theoretical framework for filtered back-projection in tomosynthesis," *Proc. SPIE* **3338**, 1127–1137 (1998).
- ²⁰H. Matsuo, A. Iwata, I. Horiba, and N. Suzumura, "Three-dimensional image reconstruction by digital tomosynthesis using inverse filtering," *IEEE Trans. Med. Imaging* **12**, 307–313 (1993).
- ²¹Y. Chen, J. Lo, and J. T. Dobbins III, "Matrix inversion tomosynthesis (MITS) of the breast: Preliminary results," in *RSNA 90th Scientific Assembly*, Chicago, IL, 2004.
- ²²J. T. Dobbins III, "Matrix inversion tomosynthesis improvements in longitudinal x-ray slice imaging (U.S. Patent #4,903,204)," Duke University, United States, 1990.
- ²³D. J. Godfrey, R. L. Warp, J. T. Dobbins III, "Optimization of matrix inverse tomosynthesis," *Proc. SPIE* **4320**, 696–704 (2001).
- ²⁴D. J. Godfrey, H. P. McAdams, and J. T. Dobbins III, "Optimization of the matrix inversion tomosynthesis (MITS) impulse response and modulation transfer function characteristics for chest imaging," *Med. Phys.* **33**, 655 (2006).
- ²⁵M. Bissonnette, M. Hansroul, E. Masson, S. Savard, S. Cadieux, P. War-moes, D. Gravel, J. Agopyan, B. T. Polischuk, W. H. Haerer, T. Mertelmeier, J. Y. Lo, Y. Chen, J. T. Dobbins III, J. L. Jesneck, and S. Singh, "Digital breast tomosynthesis using an amorphous selenium flat panel detector," *Proc. SPIE* **5745**, 529–540 (2005).
- ²⁶E. Samei, J. T. Dobbins III, J. Y. Lo, and M. P. Tornai, "A framework for optimizing the radiographic technique in digital x-ray imaging," *Radiation Protection Dosimetry* (Oxford University Press, Oxford, 2005).
- ²⁷Y. Chen, J. Y. Lo, N. T. Ranger, E. Samei, and J. T. Dobbins III, "Methodology of NEQ(f) analysis for optimization and comparison of digital breast tomosynthesis acquisition techniques and reconstruction algorithms," *Proc. SPIE* **6510**, 65101-I (2007).
- ²⁸Y. Chen, J. Y. Lo, J. T. Dobbins III, "Two-dimensional shift-and-add algorithm for digital breast tomosynthesis reconstruction," *Med. Phys.* **33**, 2001 (2006).

A comparison between traditional shift-and-add (SAA) and point-by-point back projection (BP) -- relevance to morphology of microcalcifications for isocentric motion in Digital Breast tomosynthesis (DBT)

^{a, b, c}Ying Chen, ^{b, c, d}Joseph Y. Lo, ^{b, c, d}James T. Dobbins III

^a*Department of Electrical and Computer Engineering,
Southern Illinois University Carbondale, Carbondale, IL 62901*

^b*Department of Biomedical Engineering*

^c*Duke Advanced Imaging Laboratories*

^d*Medical Physics Graduate Program*

Duke University and Duke University Medical Center

Durham, North Carolina 27710

ada_yingchen@yahoo.com

Abstract

Digital breast tomosynthesis (DBT) is a three-dimensional imaging technique providing an arbitrary set of reconstruction planes in the breast with limited series of projection images. This paper describes a comparison between traditional shift-and-add (SAA) and point-by-point back projection (BP) algorithms by impulse response and modulation transfer function (MTF) analysis.

Due to the partial isocentric motion of the x-ray tube in DBT, structures such as microcalcifications appear slightly blurred in traditional shift-and-add (SAA) images in the direction perpendicular to the direction of tube's motion. Point-by-point BP improved rendition of microcalcifications. The sharpness and morphology of calcifications were improved in a human subject images. A Filtered Back Projection (FBP) deblurring approach was used to demonstrate deblurred point-by-point BP tomosynthesis images. The point-by-point BP rather than traditional SAA should be considered as the foundation of further deblurring algorithms for DBT reconstruction.

1. Introduction

Breast cancer is second only to lung cancer as the leading cause of non-preventable cancer death. Digital

breast tomosynthesis (DBT) has been considered as a promising technique to improve early breast cancer detection. Compared with standard mammography two-dimensional imaging techniques, digital breast tomosynthesis (DBT) three-dimensional imaging methods improve conspicuity of structures by removing the visual clutter associated with overlying anatomy [1,2,3,4,11]. Several tomosynthesis image reconstruction algorithms have been proved effectively in DBT image reconstruction at of yet, including traditional shift-and-add (SAA) [1,2], Niklason and colleagues' image stretching shift-and-add [3], Wu *et al*'s maximum likelihood maximization expectation (MLEM) [4,5], tuned-aperture computed tomography (TACT) [6,7], filtered back projection [2,16-19], matrix inversion tomosynthesis [2,8,12], algebraic reconstruction techniques (ART) [14], and Gaussian frequency blending (GFB) of MITS and FBP [9].

Traditional shift-and-add (SAA) is a common mathematical algorithm to calculate the shift-amount along x-ray tube's motion direction to line up in-plane structures and suppress out-of-plane artifacts [1,2]. It has been served as the basis for a few other algorithms such as Niklason and colleagues' image stretching SAA [3], TACT [6,7], MITS [2,8], etc. With isocentric motion of DBT, the shift amount doesn't fall into a plane parallel to tube's motion plane [10]. It actually occurs in both x-ray tube's motion and the motion

perpendicular to tube motion direction. As a result, structures such as microcalcifications appear slightly blurred.

This paper compared the impulse responses and modulation transfer function (MTF) of traditional SAA and a point-by-point back projection (BP) algorithm. Geometries of a Siemens selenium-based direct conversion Mammomat Novation prototype system were used to simulate tomosynthesis projection images. Reconstructed region of interests (ROI) of microcalcification of a human subject were evaluated. A FBP deblurring algorithm based on point-by-point BP was further investigated to demonstrate deblurred BP tomosynthesis images, as they would normally be portrayed to observers.

Results showed that point-by-point BP improved the sharpness and morphology of microcalcifications especially in the direction perpendicular to tube's motion direction. The FBP deblurring algorithm based on point-by-point BP provided good rendition of detailed structures, reduced out-of-plane blur, and suppressed high frequency noise. Point-by-point BP rather than traditional SAA should be considered as the basis of further deblurring algorithms to improve the sharpness and morphology of structures especially for small objects such as calcifications. This may prove helpful to radiologists in discriminating malignant from benign microcalcification patterns, and thereby improve the accuracy of breast cancer detection.

2. Methods

Figure 1 shows a breast tomosynthesis imaging acquisition system [11] modified from a selenium-based Siemens Mammomat Novation prototype system. The x-ray tube moves along an arc above the digital detector. The actually angular range of the x-ray tube can be up to $\pm 25^\circ$ at the rotation center that is 60 mm above the detector surface. The pixel size is $85 \mu\text{m}$. It takes around 20 seconds for a typical tomosynthesis sequence acquisition with 25 projection images.

Geometries of Siemens tomosynthesis imaging acquisition system were used to simulate tomosynthesis projection images. In this paper, a single delta function located at 40 mm above the detector surface cover was simulated as the input impulse to evaluate impulse responses and modulation transfer function (MTF) of traditional SAA and point-by-point BP. Tomosynthesis sequence datasets of the impulse were simulated by ray-tracing method for 49 projection images and $\pm 25^\circ$

x-ray tube angular range with respect to the rotation center.



Figure 1. Siemens tomosynthesis imaging device

Two different locations of simulated impulses were considered: 1) the impulse was located 4 cm away from the chest wall (front edge of the detector) and 40 mm above the detector surface cover; 2) the impulse was located near the chest wall (only 20 pixels in distance) and 40 mm above the detector surface cover. Shading background effects of $1/r^2$ exposure variation (r is the distance from the projection point to the x-ray point source) was taken into account. Projection images for shading background only and impulse-added were simulated separately.

When the x-ray tube moves, objects at different heights above the detector will be projected onto the detector at different positions according to the relative heights of the objects [1]. In order to reconstruct slice images of the breast at a certain height above the detector, each projection image should be shifted by an amount appropriate for the plane of reconstruction. Based on the projected locations of the central point on each projection image, traditional shift-and-add (SAA) shifts each projection plane one-dimensionally along tube's motion direction. The shifted planes were added together to emphasize structures in in-focus plane and blur out structures in other planes [2]. Point-by-point BP calculates the exact two-dimensional projected location for each pixel on reconstructed planes at a certain height above the detector. All involved image values on contributing projection images were then added together and back projected to generate reconstruction images [5, 10, 20].

The simulated tomosynthesis datasets of projection images were then reconstructed by traditional SAA and point-by-point BP algorithms. The image size is 2048 * 2048 with a pixel size of 85 μm . A reconstruction slice thickness of 5 mm was used. In order to eliminate background shading effects, reconstruction images from background-only projections were subtracted from reconstructions of impulse-added projections. In-plane impulse responses on the reconstruction plane (40 mm above the detector surface cover) and out-of-plane responses (35 mm above the detector surface cover) were analyzed and compared. The impulse responses were normalized based on the ideal condition when the impulse is exactly located underneath the x-ray source. Modulation Transfer Function (MTF) was computed as normalized two-dimensional Fourier Transform of the impulse responses at reconstruction planes.

3. Results

Figures 2, 3, 4, and 5 show impulse response and MTF results of traditional SAA and point-by-point BP for simulated tomosynthesis projection images of 49 projection images and $\pm 25^\circ$ x-ray tube angular range (with respect to the rotation center). Figures 2 and 3 are results from traditional SAA and point-by-point BP respectively when the impulse was located 40 mm above the detector surface cover and about 4 cm away from the chest wall. Figures 4 and 5 are results when the impulse was located 40 mm above the detector surface plate and near the chest wall. In figures 2 through 5, (a) and (b) represent the out-of-plane responses in a reconstruction plane that is 5 mm below the impulse's location; (c) and (d) represent the in-plane responses in a reconstruction plane that is exactly at the impulse's location. In (a) and (c), the normalized amplitude of impulse responses were displayed. The x and y axes represent the pixel location on the reconstruction plane. y direction is the x-ray tube's motion direction. Only a 40×40 pixels region close to the impulse was shown for clarity. In (b) and (d), MTF curves were displayed with u and v axes representing spatial frequencies conjugate to x and y .

When the impulse was located 4 cm away from chest wall, the in-plane response of traditional SAA is noticeably blurred in the x direction that is perpendicular to the direction of tube motion (figure 2c). The out-of-plane artifacts appeared curved for traditional SAA, reflecting the uncorrected partial isocentric tube motion (figure 2a). Point-by-point BP

provides sharper in-plane response without x direction blur (figure 3c). The out-of-plane response changed from curved to be straight (figure 3a). Compared with that of traditional SAA (figure 2b), the MTF performance of point-by-point BP is much smoother (figure 3b).

When the impulse was located close to chest wall, no substantial difference between traditional SAA and point-by-point BP was noticed. However, one can still find that the in-plane response of point-by-point BP is a little sharper by giving a higher magnitude of the impulse response (figures 4c vs 5c).

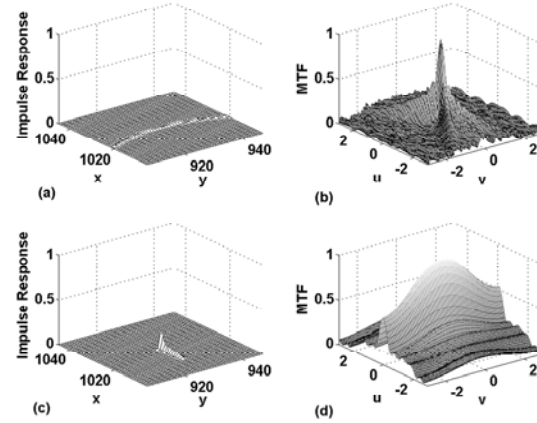


Figure 2. Traditional SAA impulse response and MTF, impulse located about 4 cm away from the chest wall. (a) and (b) give the impulse response and MTF, respectively, at a reconstruction plane 5 mm below the impulse location; (c) and (d) give corresponding values in a plane at the exact height of the impulse's location.

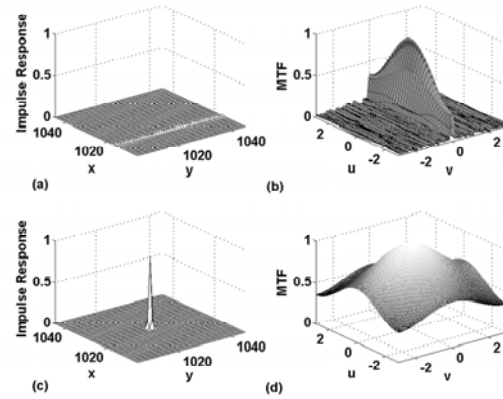


Figure 3. Point-by-point BP impulse response and MTF, impulse located about 4 cm away from the

chest wall. (a) and (b) give the impulse response and MTF, respectively, at a reconstruction plane 5 mm below the impulse location; (c) and (d) give corresponding values in a plane at the exact height of the impulse's location.

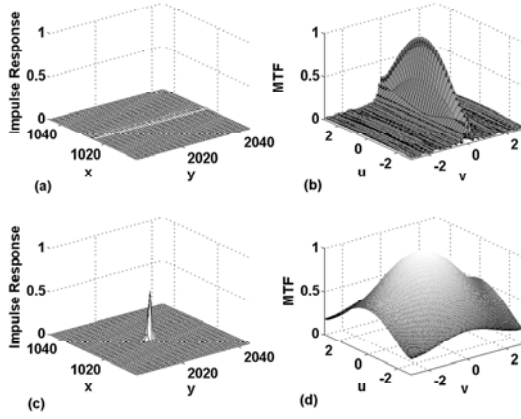


Figure 4. Traditional SAA impulse response and MTF, impulse located near the chest wall. (a) and (b) give the impulse response and MTF, respectively, at a reconstruction plane 5 mm below the impulse location; (c) and (d) give corresponding values in a plane at the exact height of the impulse's location.

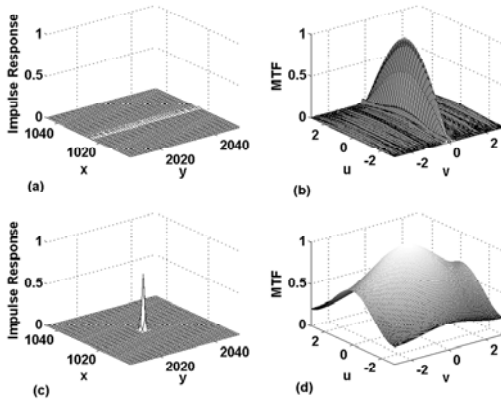


Figure 5. Point-by-point BP impulse response and MTF, impulse located near the chest wall. (a) and (b) give the impulse response and MTF, respectively, at a reconstruction plane 5 mm below the impulse location; (c) and (d) give corresponding values in a plane at the exact height of the impulse's location.

The tomosynthesis projection images of human subjects have been acquired on our prototype breast

tomosynthesis system (figure 1) under an IRB-approved protocol. Figure 6 shows a reconstructed $7.99 \text{ mm} \times 7.99 \text{ mm}$ region of interest (ROI) of a human subject breast containing a round-shaped calcification. The tomosynthesis sequence was acquired with 25 projection images and $\pm 25^\circ$ angular range at the rotation center. The tomosynthesis technique of W/Rh at 28 kVp and 112 mAs was used to maintain the same dose as the conventional left cranio caudal (LCC) mammogram of the human subject.

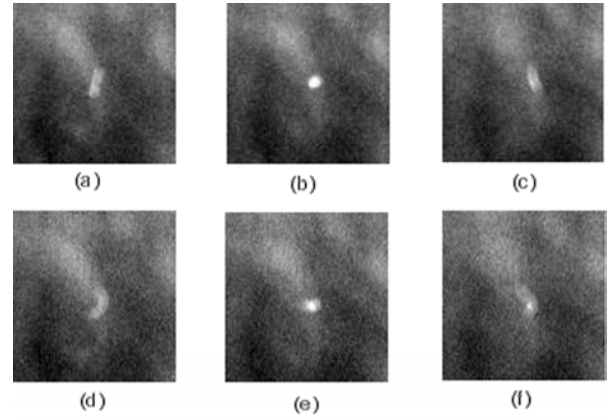


Figure 6. Reconstructed $7.99 \text{ mm} \times 7.99 \text{ mm}$ ROI of a human breast containing a calcification: (a) point-by-point BP, $Z=25.5 \text{ mm}$; (b) point-by-point BP, $Z=27 \text{ mm}$; (c) point-by-point BP, $Z=28.5 \text{ mm}$; (d) traditional SAA, $Z=25.5 \text{ mm}$; (e) traditional SAA, $Z=27 \text{ mm}$; (f) traditional SAA, $Z=28.5 \text{ mm}$.

In figure 6, $Z=27 \text{ mm}$ represents the in-plane reconstruction of the round-shaped calcification. Figures (a) and (d) represent the out-of-plane reconstruction that is 1.5 mm below the in-plane location. (c) and (f) are reconstruction regions that is 1.5 mm above the in-plane location. Compared with traditional SAA (figure 6e), edges of calcifications are sharper and better focused with point-by-point BP (figures 6b). With traditional SAA, out-of-plane structures were blurred and had curved appearance (figures 6d and 6f). With 2D-SAA, those problems were corrected, and the out-of-plane structures appear as straight line segments (figures 6a and 6c).

Figure 7 shows a low dose middle projection image of the same human breast when the x-ray tube was positioned at the middle (0°) position. Figure 8 shows reconstructed slice image at a height of 16.5 mm above the detector surface cover by a deblurring FBP based

on point-by-point BP. It applies a deblurring ramp filter to projection images and point-by-point back projects the filtered projections to generate reconstruction images [2,9]. A Hamming filter and a Gaussian filter was further applied to control high frequency noise [9].

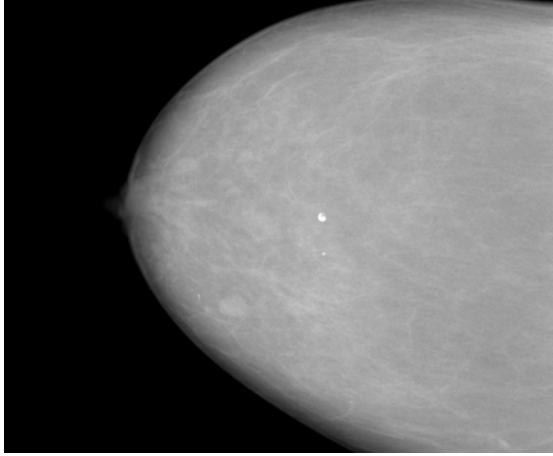


Figure 7. Low dose middle (0°) projection

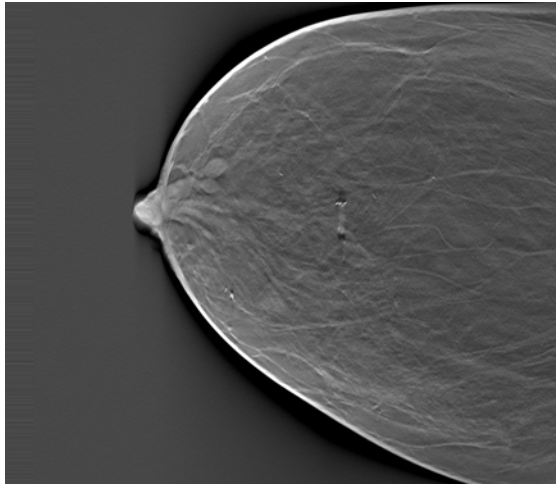


Figure 8. FBP reconstruction slice based on Point-by-point BP

Compared with low dose middle projection that is similar to a two-dimensional standard mammography image, tomosynthesis reconstruction images provided better appearance of the breast with depth information.

The FBP deblurred point-by-point BP image (Fig. 8) demonstrates good rendition of breast anatomy out to the skin line and provided good rendition of detailed structures and suppressed high frequency noise.

4. Discussion

Due to isocentric motion of x-ray tube in DBT, the track of projected locations of objects occurs in both tube's motion direction and a direction perpendicular to tube's motion direction. Traditional SAA calculates shift amount for each projection image only along the tube's motion direction. As a result, the in-plane structures are blurred. Illustrations with impulse responses, MTF, and reconstructed human subject images showed that this is an inherent problem of traditional SAA with breast tomosynthesis. Traditional SAA can tolerate when the impulse was close to the chest wall. However, when the object was farther away from the chest wall, problem existed with $\pm 25^\circ$ angular range. Therefore, with traditional SAA, objects such as microcalcifications appear slightly blurred in the direction perpendicular to the direction of tube motion, and their morphology changes.

The morphology of calcifications coming from the isocentric x-ray tube's movement is corrected with point-by-point BP algorithm. The in-plane structures are sharper. Isocentric motion of x-ray tube in DBT also introduces variable magnification. The magnification of objects at different heights above the detector varies from plane-to-plane. Even within the same reconstruction plane, the magnification also changes at different pixel locations. Therefore, the reconstructed size of an object by traditional SAA doesn't reflect the real size of the object. Point-by-point calculates shift amount for each pixel according to the exact location of the pixel in the reconstruction slices, thereby, addressing this issue of variable magnification.

To evaluate, whether deblurring filters gave reasonable results with point-by-point BP (even though not perfectly spatially invariant), a FBP reconstruction with applied deblurring filters to point-by-point BP images was illustrated. Although not completely spatially invariant, this approach subjectively did a good job of effective deblurring with point-by-point BP and was relatively fast. Results with human subjects demonstrated subjectively that FBP deblurring with point-by-point BP provides good rendition of detailed structures, reduced out-of-plane blur, and suppressed high frequency noise. Other deblurring algorithms, such as Matrix Inversion Tomosynthesis (MITS) [2, 8], may also prove effective, though not perfectly, in this spatially non-invariant environment, and will be investigated in the future.

5. Conclusion

This paper demonstrates the importance of using a point-by-point BP correction of isocentric motion artifacts in tomosynthesis imaging of the breast, where the morphology of microcalcifications bears a significant meaning on clinical decision making. Compared with traditional SAA, point-by-point BP improves the sharpness and rendition of morphology of structures such as microcalcifications. Point-by-point BP provides better-focused in-plane response and less curvature artifacts. Issues of variable magnifications associated with isocentric motion of DBT are also addressed by point-by-point BP. Our example of FBP reconstructions based on point-by-point BP shows better rendition of breast anatomy and good rendition of detailed structures and suppressed out-of-plane artifacts. The point-by-point BP rather than traditional SAA should be considered as the foundation for further deblurring algorithms such as FBP.

Acknowledgments

We thank Jay A. Baker, M.D., at Duke University Medical Center for clinical insight and helpful discussion. This work was supported by a grant from US Army Breast Cancer Research Program (USAMRMC W81XWH-06-1-0462), a research grant from Siemens Medical Solutions, and NIH/NCI R01 112437.

References

- [1] J. T. Dobbins, III., D. J. Godfrey, "Digital X-ray tomosynthesis: current state of the art and clinical potential", *Phys. Med. Biol.*, vol. 48, 2003, pp 65-106.
- [2] Y. Chen, J. Y. Lo, J. T. Dobbins III, "Impulse response analysis for several digital tomosynthesis mammography reconstruction algorithms", *Proc. SPIE*, vol. 5745, 2005, pp 541-549.
- [3] L. T. Niklason, et al., "Digital tomosynthesis in breast imaging", *Radiology*, Vol. 205, 1997, pp 399-406.
- [4] T. Wu, et al., "Tomographic mammography using a limited number of low-dose cone-beam projection images", *Med. Phys.*, vol. 30, 2003, pp 365-380.
- [5] T. Wu, R. H. Moore, E. A. Rafferty, D. B. Kopans, "A comparison of reconstruction algorithms for breast tomosynthesis", *Med. Phys.*, vol 9, 2004, pp 2636-2647.
- [6] S. Suryanarayanan, A. Karellas, S. Vedantham, S. J. Glick, C. J. D'Orsi, S. P. Baker, and R. L. Webber, "Comparison of tomosynthesis methods used with digital mammography", *Acad. Radiol.*, vol. 7, 2000, pp 1085-1097.
- [7] S. Suryanarayanan, A. Karellas, S. Vedantham, S. P. Baker, S. J. Glick, C. J. D'Orsi, S. P. Baker, and R. L. Webber, "Evaluation of linear and nonlinear tomosynthetic reconstruction methods in digital mammography", *Acad. Radiol.*, vol. 8, 2001, pp 219-224.
- [8] Y. Chen, J. Lo, J. T. Dobbins III, "Matrix Inversion Tomosynthesis (MITS) of the Breast: Preliminary Results", in *RSNA 90th Scientific Assembly*, Chicago, IL, 2004.
- [9] Y. Chen, J. Y. Lo, J. A. Baker, J. T. Dobbins III, "Gaussian frequency blending algorithm with Matrix Inversion Tomosynthesis (MITS) and Filtered Back Projection (FBP) for better digital breast tomosynthesis reconstruction", *Proc. SPIE*, vol. 6142, 2006, pp 122-130.
- [10] Y. Chen, J. Y. Lo, J. T. Dobbins III, "Two-dimensional Shift-And-Add Algorithm for Digital Breast Tomosynthesis Reconstruction", *Med. Phys.*, vol. 33 (6), 2006, pp 2006.
- [11] M. Bissonnette, M. Hansroul, E. Masson, S. Savard, S. Cadieux, P. Warmoes, D. Gravel, J. Agopyan, B. T. Polischuk, W. H. Haerer, T. Mertelmeier, J. Y. Lo, Y. Chen, J. T. Dobbins III, J. L. Jesneck, S. Singh, "Digital breast tomosynthesis using an amorphous selenium flat panel detector", *Proc. SPIE*, vol. 5745, 2005, pp 529-540.
- [12] J. T. Dobbins, III, "Matrix Inversion Tomosynthesis improvements in longitudinal x-ray slice imaging (U.S. Patent #4,903,204)," Duke University, United States, 1990.
- [13] E. Samei, J. T. Dobbins III, J. Y. Lo, M. P. Tornai, "A framework for optimizing the radiographic technique in digital x-ray imaging", *Radiation Protection Dosimetry* (Oxford University Press, 2005).
- [14] Y. Zhang, H. Chan, B. Sahiner, J. Wei, M. M. Goodsitt, L. M. Hadjiiski, J. Ge, C. Zhou, "A comparative study of limited-angle cone-beam reconstruction methods for breast tomosynthesis", *Med. Phys.*, vol. 33(10), 2006, pp 3781-3795.
- [15] L. Zhou, J. Oldan, P. Fisher, and G. Gindi, "Low-contrast lesion detection in tomosynthetic breast imaging using a realistic breast phantom", *Proc. SPIE*, vol. 6142, 2006, pp 1685-1696.
- [16] T. Mertelmeier, J. Orman, W. Haerer, and M. K. Dudam, "Optimizing filtered backprojection reconstruction for a breast tomosynthesis prototype device", *Proc. SPIE*, vol. 6142, 2006, pp 131-142.
- [17] G. M. Stevens, R. Fahrig and N. J. Pelc, "Filtered backprojection for modifying the impulse response of circular tomosynthesis", *Med. Phys.*, vol. 28, 2001, pp 372-380.

- [18] G. Lauritsch and W. Haerer, "A theoretical framework for filtered back-projection in tomosynthesis", *Proc. SPIE*, vol. 3338, 1998, pp 1127-1137.
- [19] Hiroshi Matsuo, Akira Iwata, Isao Horiba, Nobuo Suzumura, "Three-dimensional image reconstruction by digital tomo-synthesis using inverse filtering", *IEEE Trans. Med. Imaging*, vol. 12, 1993, pp 307-313.
- [20] Y. Chen, J. Y. Lo, and J. T. Dobbins III., "Importance of point-by-point Back Projection (BP) correction for isocentric motion in digital breast tomosynthesis: relevance to morphology of microcalcifications," manuscript, submitted to *Med. Phys.*, in review, 2007.

Medical Physics Online

[Current Issue: [Browse](#) | [Search](#)] - [All Online Issues: [Browse](#) | [Search](#)]
 [[Entry Page](#)] - [SPIN database: [Search](#)] - [[Purchase Articles Online](#)]
 [[Journal Homepage](#)] - [[Scitation Home](#)] - [[Feedback](#)] - [[HELP](#)] - [[EXIT](#)]



[[Previous](#) / [Next](#) Abstract | [Issue Table of Contents](#) | [Bottom of Page](#)]

**Medical Physics -- June 2006 -- Volume 33,
Issue 6, p. 2001**

Options for selected Articles [View MyArticles](#) [?](#)

Choose an action

Select up to 20 articles at a time. [YOUR CART](#)

Full Text: [[PDF](#) (4168 kB) [GZipped PS](#)] [Order](#)

SU-FF-I-21: Two-Dimensional Shift-And-Add (SAA) Algorithm for Digital Breast Tomosynthesis Reconstruction

[Y Chen](#), [J Lo](#), [J Baker](#), and [J Dobbins](#)

Duke University, Durham, NC

Duke University Medical Center, Durham, NC

Purpose: To investigate a two-dimensional Shift-And-Add algorithm for three-dimensional digital breast tomosynthesis reconstruction to correct for defects existing in the traditional Shift-And-Add algorithm that calculates only one-dimensional shift amount along the axis of x-ray tube's motion.

Method and Materials: With the traditional Shift-And-Add (SAA) algorithm for breast tomosynthesis reconstruction, shift amounts for each projection plane are calculated only along the axis of x-ray tube's movement. As a result, small objects such as microcalcifications appear slightly blurred in the direction perpendicular to the direction of tube motion. In this project, a two-dimensional SAA method was developed to correct for this phenomenon. Shift amounts for every pixel location on each reconstruction plane were computed, taking into account the 2D arc projection location of reconstructed objects in each plane. Bilinear interpolation was used for partial pixel locations. Impulses at different 3-D locations were simulated and a few human subject tomosynthesis sequences were acquired for investigation.

Results: Two-dimensional SAA demonstrated the improvement in the direction that is perpendicular to the tube motion direction. For human subjects, the appearance of calcifications from 2D SAA was sharper than traditional SAA at the direction orthogonal to the tube motion direction. The out-of-plane artifacts of calcifications changed from curved to be straight. **Conclusion:** Two-dimensional SAA is an effective method to reconstruct 3D tomosynthesis images of the breast. Compared with the traditional SAA, the new method corrects for 2D shift amounts coming from the isocentric tube motion. This provides more accurate and reliable results compared with other SAA algorithms. **Conflict of Interest:** Research sponsored in part by a research grant from Siemens Medical Solutions. ©2006 *American Association of Physicists in Medicine*

Methodology of NEQ (f) analysis for optimization and comparison of digital breast tomosynthesis acquisition techniques and reconstruction algorithms

Ying Chen^{a,b}, Joseph Y. Lo^{a,b,c,d}, Nicole T. Ranger^{b,c}, Ehsan Samei^{a,b,c,d}, James T. Dobbins III^{a,b,c,d}

^aDepartment of Biomedical Engineering, Duke University, Durham, NC, USA 27710

^bDuke Advanced Imaging Laboratories, Duke University Medical Center, Durham, NC, USA 27710

^cDepartment of Radiology, Duke University Medical Center, Durham, NC, USA 27710

^dMedical Physics Graduate Program, Duke University Medical Center, Durham, NC, USA 27710

ABSTRACT

As a new three-dimensional imaging technique, digital breast tomosynthesis allows the reconstruction of an arbitrary set of planes in the breast from a limited-angle series of projection images. Though several tomosynthesis algorithms have been proposed, no complete optimization and comparison of different tomosynthesis acquisition techniques for available methods has been conducted as of yet. This paper represents a methodology of noise-equivalent quanta NEQ (f) analysis to optimize and compare the efficacy of tomosynthesis algorithms and imaging acquisition techniques for digital breast tomosynthesis. It combines the modulation transfer function (MTF) of system signal performance and the noise power spectrum (NPS) of noise characteristics. It enables one to evaluate the performance of different acquisition parameters and algorithms for comparison and optimization purposes. An example of this methodology was evaluated on a selenium-based direct-conversion flat-panel Siemens Mammomat Novation prototype system. An edge method was used to measure the presampled MTF of the detector. The MTF associated with the reconstruction algorithm and specific acquisition technique was investigated by calculating the Fourier Transform of simulated impulse responses. Flat field tomosynthesis projection sequences were acquired and then reconstructed. A mean-subtracted NPS on the reconstructed plane was studied to remove fixed pattern noise. An example of the application of this methodology was illustrated in this paper using a point-by-point Back Projection correction (BP) reconstruction algorithm and an acquisition technique of 25 projections with 25 degrees total angular tube movement.

Keywords: mammography, tomosynthesis, breast imaging, modulation transfer function (MTF), noise power spectrum (NPS), Noise-equivalent quanta (NEQ), impulse response, Back Projection (BP)

1. INTRODUCTION

Digital breast tomosynthesis is a new technique to reconstruct an arbitrary set of planes in the breast from a limited-angle series of projection images when the x-ray source moves along an arc above the breast. As of yet, several tomosynthesis algorithms have been proposed [3,4,10-22], including Shift-And-Add (SAA) [3,4], Niklason and colleagues' publication in 1997 of a tomosynthesis method with the x-ray tube moved in an arc above the stationary breast and detector [10], Wu et al.'s report in 2003 of the maximum likelihood iterative algorithm (MLEM) to reconstruct the three-dimensional distribution of x-ray attenuation in the breast [11], and the filtered back projection (FBP) algorithms [12,13,18-24], tuned-aperture computed tomography (TACT) reconstruction methods developed by Webber and investigated by Suryanarayanan *et al* [16], algebraic reconstruction techniques (ART) [14,23,24], filtered back projection (FBP) [4,13,18-21], matrix inversion tomosynthesis (MITS) [15,26] and Gaussian Frequency Blending (GFB) algorithm to combine the MITS and FBP for better reconstruction [22].

The selection of optimal acquisition parameters and reconstruction algorithm plays an important role in producing better performance. However, there are several factors involved in this task and some of them are not individually independent. An effective methodology will enable one to optimize selection of acquisition parameters and compare algorithms for various digital breast tomosynthesis methods. Recently, Godfrey et al. proposed methods of MTF and NPS measurement to quantitatively characterize the optimal acquisition parameters selection for chest tomosynthesis application^[6,7]. In 2005 and 2006, we also published the impulse response and NPS analysis for different acquisition parameters and reconstruction algorithms^[3,4].

In this paper, a methodology of NEQ (f) analysis is proposed to optimize and compare the efficacy of tomosynthesis algorithms and imaging acquisition techniques for digital breast tomosynthesis. It combines the modulation transfer function (MTF) of system signal performance and the noise power spectrum (NPS) of noise characteristics. It enables one to evaluate the performance of different acquisition parameters and algorithms for comparison and optimization purposes.

2. METHODS

The NEQ (f) is defined as: $NEQ(f) = \frac{MTF^2(f)}{NNPS(f)}$. The modulation transfer function (MTF) and the normalized noise power spectrum (NNPS) are included to evaluate the performance of the reconstruction algorithms and the acquisition techniques. The normalized NPS (NNPS) is defined as: $NNPS(u, v) = \frac{NPS_{tomo}(u, v)}{gain^2}$ due to the logarithmic transform in digital tomosynthesis. Hence, the NEQ (f) can be calculated by: $NEQ(f) = \frac{gain^2 \cdot MTF^2(f)}{NPS_{tomo}(f)}$. In digital breast tomosynthesis reconstruction, the step of logarithmic transform involved, and therefore, the determination of NEQ (f) is more similar to that of a screen-film system than to a linear digital detector.

2.1 MTF measurement

The MTF measurement includes two parts: 1) the system MTF of the detector; 2) the reconstruction MTF associated with specific reconstruction algorithm and acquisition parameters.

2.1.1 System MTF Measurement

The system MTF describes the measured MTF of the detector. An edge method was applied at a range of tube angles to see if there is any difference with angle. In this paper, five different angular positions of 0° , $\pm 15^\circ$, and $\pm 25^\circ$ of the X-ray tube were selected as the representative angles.

Table 1 shows the MW2^[8] technique we used for the system MTF measurement.

Technique	Acquisition Mode	kV	Spectrum	Number of views (N)	Total mAs	mAs for a single projection
MW2	B0XD11 (slow speed)	28	W/Rh	11	303	≈ 27.5

Table 1. System MTF measurement technique

Figure 1 shows the set up of the system MTF measurement experiment. A 0.1mm Pt-Ir edge was placed in contact with the detector and oriented at a $1^\circ \sim 3^\circ$ angle with respect to the pixel array. Edge images were then acquired with MW2 technique and 2mm Aluminum filtration. A previously published routine^[8,9] was used to analyze the edge images in a region around the edge (ROI=256*256 pixels, pixel size=85 μ m) to compute the presampled system MTF.

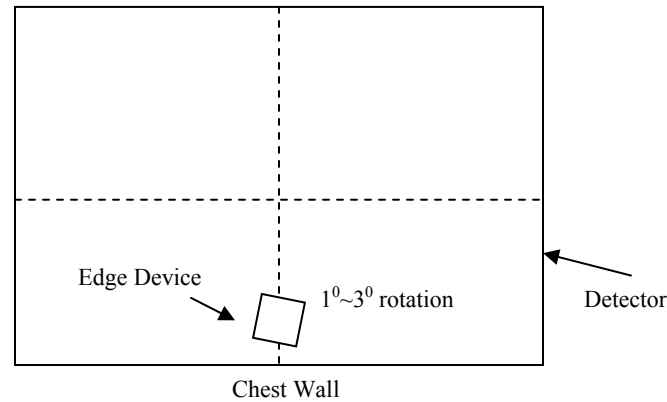


Figure 1. Set up of system MTF measurements

2.1.2 Reconstruction MTF measurement

The reconstruction MTF describes the calculated MTF associated with specific algorithm and acquisition parameters. A dataset of tomosynthesis projection images of a simulated delta function with the specific acquisition parameters was served as the input signal. A ray-tracing simulation method was used to project the single delta function onto the detector to simulate the tomosynthesis sequence of projection images. Figure 2 shows the ray-tracing method to simulate the projection images of a delta function.

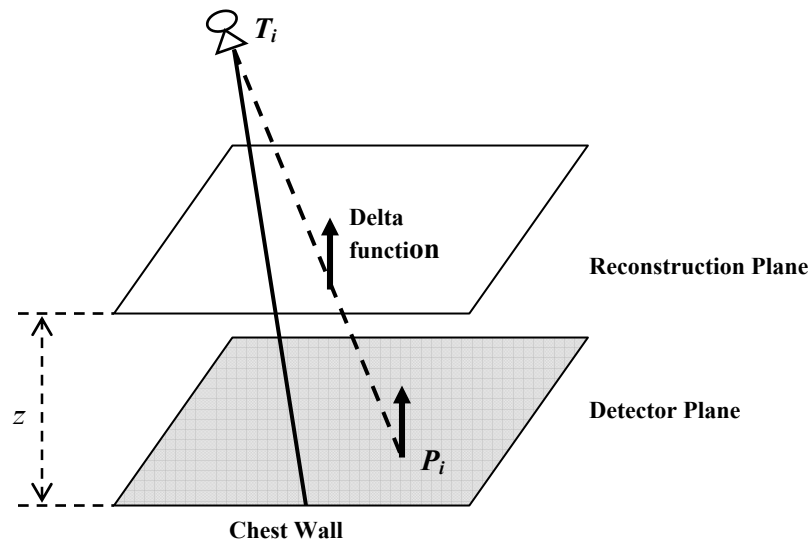


Figure 2. Ray-tracing simulation

In Figure 2, a single delta function at z distance above the detector was simulated. The delta function is projected onto the detector at P_i when the x-ray tube moves to T_i location. Partial pixel sharing was performed if P_i falls into non-integer pixel location. With this ray-tracing method, for a specific group of acquisition parameters, a dataset of projection images from different x-ray tube locations can be simulated.

Projection images with $1/r^2$ background and without background were considered, where r is the distance between the x-ray source T_i and the pixel location P_i on each projection image. Datasets of simulated projection images with $1/r^2$ background and without background were separately reconstructed by the specific reconstruction algorithm. The reconstruction images without background were then subtracted from the reconstruction images with background to get rid of effects associated with the $1/r^2$ background ray-tracing simulation.

The reconstruction MTF can be computed as the Fourier Transform of the point spread function (PSF) on the reconstruction plane where the simulated delta function is located (z distance above the detector).

2.1.3 Total MTF

The total MTF involves two parts as described in 2.1.1 and 2.1.2. It can be calculated as the multiplication of measured system MTF (2.1.1) and the reconstruction MTF associated with reconstruction algorithm and acquisition parameters (2.1.2). Linear interpolation was performed to match the frequency axes of the system MTF and reconstruction MTF for multiplication.

2.2 NPS measurement

In order to compute the noise power spectrum (NPS) for specific acquisition parameters, two phantom slabs of BR12 (47% water/ 53% adipose equivalent) for a total of 4 cm thickness were put directly on the detector cover to mimic the breast tissue equivalent attenuation and scattered radiation. Ten identical tomosynthesis sequences of flat images with the phantom slabs on the detector were acquired. The tomosynthesis sequences were then reconstructed.

Mean-subtracted reconstruction image data were analyzed and compared on a reconstruction plane with the same height (z distance above the detector) as described in the reconstruction MTF measurement (2.1.2). The purpose of studying mean-subtracted NPS is to remove fixed pattern noise, including structured noise and system artifacts. A previously published method^[1,2] was applied using 64 ROIs of size 128×128 to examine the noise response.

2.3 Gain factor calculation

In order to normalize NPS and fairly compare different reconstruction algorithms and acquisition parameters, the gain factor should be included in the NEQ (f) calculation.

For an x-ray screen-film imaging system, the gain factor can be considered as $gain = \log_{10}(e) \cdot \gamma$, where γ is the point slope of the film density-log x-ray fluence function^[28,29]. Figure 3 shows a typical screen-film nonlinear response to exposure. Q represents the number of incident quanta / mm^2 . From this nonlinear response curve, one can calculate the point slope γ for a specific $\log(Q)$ on this response curve.

With digital tomosynthesis, the gain factor varies with different reconstruction algorithms and acquisition techniques. In this paper, we focus on the relative NEQ (f) methodology of a single algorithm and will not include the gain factor calculation. The gain factor will be computed in future work where we will actually compare different algorithms against one another.

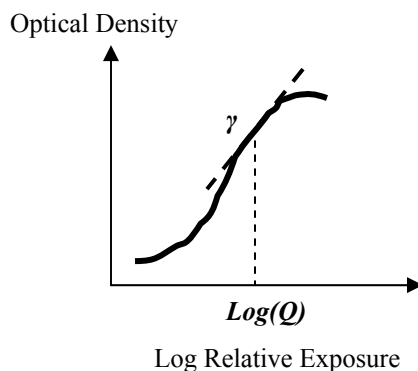
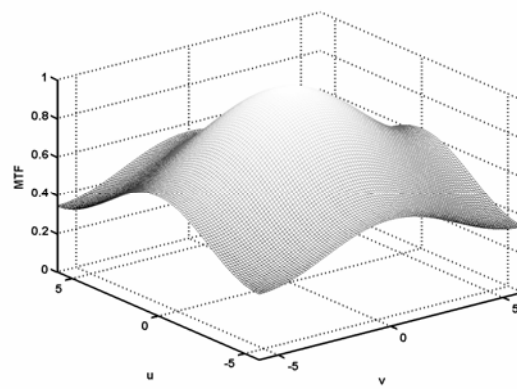
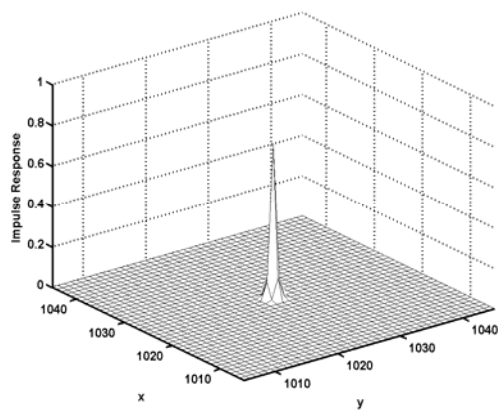
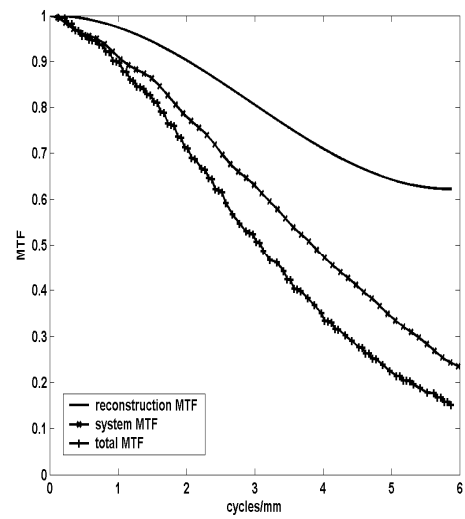
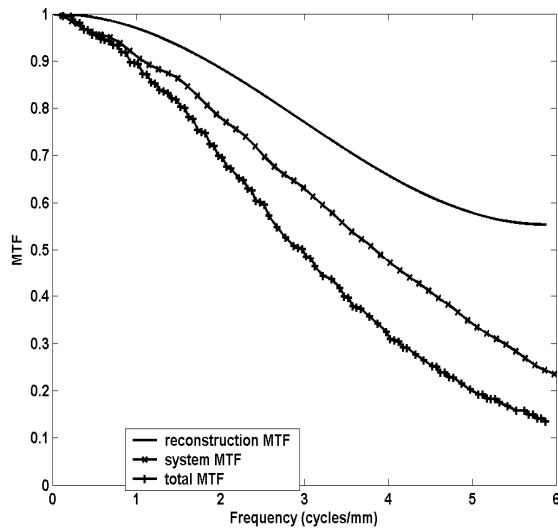
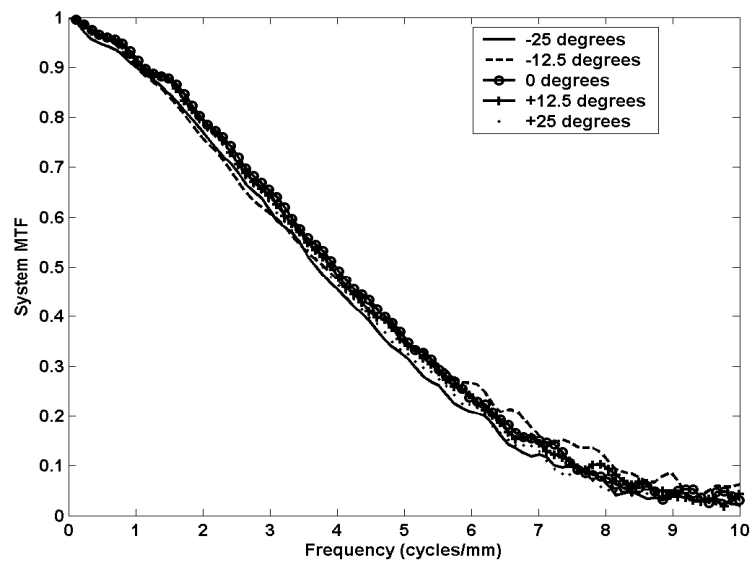
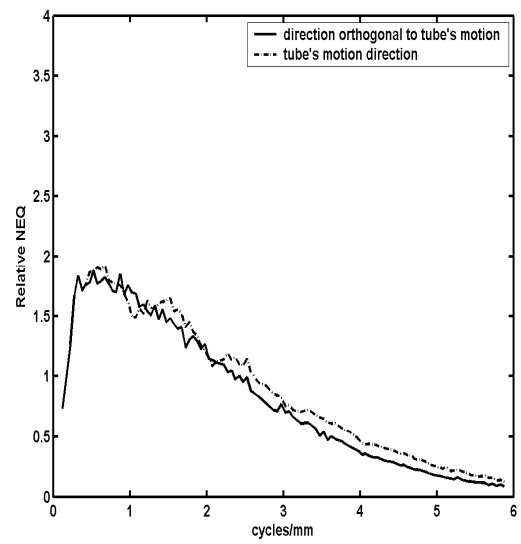
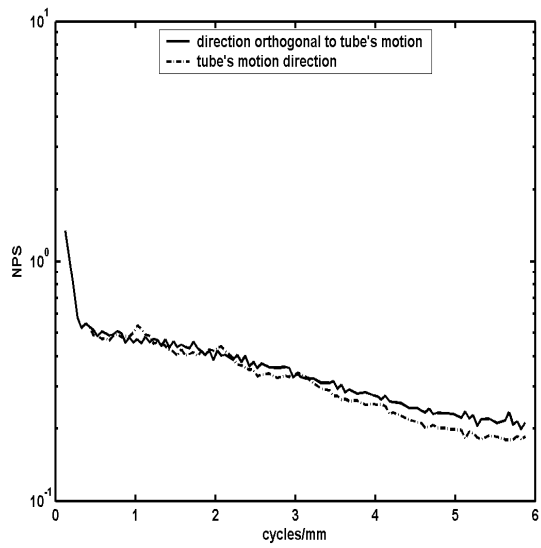


Figure 3. Screen-film characteristic curve







REFERENCE

1. J. T. Dobbins III, D.L. Ergun, L. Rutz, D. A. Hinshaw, H. Blume, D. c. Clark, "DQE (f) of four generations of computed radiography acquisition devices", *Med. Phys.* 22 (10): 1581-1593 (1995).
2. J. T. Dobbins III, "Image quality metrics for digital systems," in *Handbook of Medical Imaging*, edited by H.K.J. Beutel and R. V. Metter (SPIE, Washington, D.C., 2000), Vol. 1, pp. 163-222.
3. J. T. Dobbins, III., D. J. Godfrey, "Digital X-ray tomosynthesis: current state of the art and clinical potential", *Phys. Med. Biol.* 48: R65-R106 (2003).
4. Y. Chen, J. Y. Lo, J. T. Dobbins III, "Impulse response analysis for several digital tomosynthesis mammography reconstruction algorithms," *Proc. SPIE* 5745, 541-549 (2005).
5. Y. Chen, J. Y. Lo, J. A. Baker, J. T. Dobbins III, "Noise power spectrum analysis for several digital breast tomosynthesis reconstruction algorithms," *Proc. SPIE* 6142, 1677-1684 (2006).
6. D. J. Godfrey, H. P. McAdams, J. T. Dobbins III, "Stochastic noise characteristics in matrix inversion tomosynthesis (MITS)," submitted manuscript.
7. D. J. Godfrey, H. P. McAdams, J. T. Dobbins III, "Optimization of the Matrix Inversion Tomosynthesis (MITS) impulse response and modulation transfer function characteristics for chest imaging," *Med. Phys.* 33(3), 655-667 (2006).
8. R. S. Saunders, E. Samei, J. Jesneck, J. Lo, "Physical characterization of a prototype selenium-based full field digital mammography detector," *Med. Phys.* 32(2), 588-599 (2005).
9. R. S. Saunders and E. Samei, "A method for modifying the image quality parameters of digital radiographic images," *Med. Phys.* 30, 3006-3017 (2003).
10. L. T. Niklason, et al., "Digital tomosynthesis in breast imaging", *Radiology* 205: 399-406 (1997).
11. Tao Wu, et al., "Tomographic mammography using a limited number of low-dose cone-beam projection images", *Med. Phys.* 30 (3): 365-380, March 2003.
12. T. Wu, R. H. Moore, E. A. Rafferty, D. B. Kopans, "A comparison of reconstruction algorithms for breast tomosynthesis", *Med. Phys.* 9: 2636-2647 (2004).
13. T. Mertelemeier, J. Orman, W. Haerer, and M. K. Dudam, "Optimizing filtered backprojection reconstruction for a breast tomosynthesis prototype device," *Proc. SPIE* 6142, 131-142 (2006).
14. Y. Zhang, H. Chan, B. Sahiner, J. Wei, M. M. Goodsitt, L. M. Hadjiiski, J. Ge, C. Zhou, "A comparative study of limited-angle cone-beam reconstruction methods for breast tomosynthesis," *Med. Phys.* 33(10), 3781-3795 (2006).
15. Y. Chen, J. Lo, J. T. Dobbins III, "Matrix Inversion Tomosynthesis (MITS) of the Breast: Preliminary Results", RSNA 90th Scientific Assembly, Chicago, IL, 2004.
16. S. Suryanarayanan, A. Karellas, S. Vedantham, S. J. Glick, C. J. D'Orsi, S. P. Baker, and R. L. Webber, "Comparison of tomosynthesis methods used with digital mammography," *Acad. Radiol.* 7, 1085-1097 (2000).
17. A. D. Maidment, C. Ullberg, K. Lindman, L. Adelöw, J. Egerström, M. Eklund, T. Francke, U. Jordung, T. Kristoffersson, L. Lindqvist, D. Marchal, H. Olla, E. Penton, J. Rantanen, S. Solokov, N. Weber, and H. Westerberg, "Evaluation of a photon-counting breast tomosynthesis imaging system," *Proc. SPIE* 6142, 89-99 (2006).
18. D. G. Grant, "Tomosynthesis: a three-dimensional radiographic imaging technique", *IEEE Transactions on Biomedical Engineering*. BME-19: 20-28, 1972
19. Grant M. Stevens, Rebecca Fahrig and Norbert J. Pelc, "Filtered backprojection for modifying the impulse response of circular tomosynthesis", *Med. Phys.* 28: 372-380, 2001.
20. G. Lauritsch and W. Haerer, "A theoretical framework for filtered back-projection in tomosynthesis", *Proc. SPIE* 3338: 1127-1137, 1998.
21. Hiroshi Matsuo, Akira Iwata, Isao Horiba, Nobuo Suzumura, "Three-dimensional image reconstruction by digital tomo-synthesis using inverse filtering", *IEEE Trans. Med. Imaging*. 12: 307-313, 1993.
22. Y. Chen, J. Y. Lo, J. A. Baker, J. T. Dobbins III, "Gaussian frequency blending algorithm with Matrix Inversion Tomosynthesis (MITS) and Filtered Back Projection (FBP) for better digital breast tomosynthesis reconstruction," *Proc. SPIE* 6142, 122-130 (2006).

23. L. Zhou, J. Oldan, P. Fisher, and G. Gindi, "Low-contrast lesion detection in tomosynthetic breast imaging using a realistic breast phantom," *Proc. SPIE* 6142, 1685-1696 (2006).
24. J. T. Rakowski and M. J. Dennis, "A comparison of reconstruction algorithms for C-arm mammography tomosynthesis," *Med. Phys.* 33(8), 3018-3032 (2006).
25. M. Bissonnette, M. Hansroul, E. Masson, S. Savard, S. Cadieux, P. Warmoes, D. Gravel, J. Agopyan, B. Polischuk, W. Haerer, T. Mertelmeier, J. Lo, Y. Chen, J. Dobbins, J. Jesneck, S. Singh, "Digital breast tomosynthesis using an amorphous selenium flat panel detector," *Proc. SPIE* 5745, 529-540 (2005).
26. J. T. Dobbins, III., "Matrix Inversion Tomosynthesis improvements in longitudinal x-ray slice imaging", U.S. Patent #4,903,204 (1990). Assignee: Duke University.
27. Y. Chen, J. Y. Lo, J. T. Dobbins III, "Importance of point-by-point Back Projection (BP) correction for isocentric motion in digital breast tomosynthesis: relevance to morphology of microcalcifications," submitted manuscript.
28. P. C. Bunch, "Comparison of signal-to-noise ratios for some new screen-film systems," *Proc. SPIE* 486, 99-107, (1984).
29. P. C. Bunch, "Detective quantum efficiency of selected mammographic screen-film combinations," *Proc. SPIE* 1090, 67-77 (1989).
30. J. M. Boone, T. R. fewell and R. J. Jennings, "Molybdenum, rhodium, and tungsten anode spectral models using interpolating polynomials with application to mammography," *Med. Phys.* 24 (12), 1863-1874 (1997).
31. E. Samei, N. T. Ranger, J. T. Dobbins III, and Y. Chen, "Intercomparison of methods for image quality characterization: I. modulation transfer function," *Med. Phys.* 33 (5), 1454-1465 (2006).
32. J. T. Dobbins III, E. Samei, N. T. Ranger, and Y. Chen, "Intercomparison of methods for image quality characterization: II. noise power spectrum," *Med. Phys.* 33 (5), 1466-1475 (2006).